Nanometric determination of the thickness of aqueous samples for accurate molar absorption coefficients of water-soluble molecules in the mid-infrared region

Mónica V. Gutierrez-Salazar, and Victor A. Lorenz-Fonfria*

Institute of Molecular Science, Universitat de València, 46980 Paterna, Spain.

*Corresponding Author. E-mail: victor.lorenz@uv.es

Abstract

Absorption spectra of aqueous samples measured by transmission need to be acquired using very thin cells (5-50 μm) when targeting the mid-infrared (mid-IR) region, due to the strong background absorbance of liquid water. The thickness of the cell used controls the pathlength of the light through the sample, a value needed for instance to transform absorption spectra into molar absorption coefficient spectra, or to determine solute concentrations from absorption spectra. The most accurate way to determine the thickness of a thin empty cell (i.e., filled with air) is from the period of an interference pattern, known as interference fringes, that arises when the cell is placed perpendicular to the path of light in the spectrometer. However, this same approach is not directly applicable to determine the thickness of a cells filled with an aqueous solution, due partially to the smaller amplitude of the interference fringes but fundamentally caused by its complex waveform, with a wavenumber-dependent oscillation period. Here, using Fresnel equations, we derived analytical expressions to model interference fringes in absorption spectra obtained by transmission, valid also for aqueous samples. We also present a novel Fourier-based analysis of the interference fringes that, in combination with the derived analytical expressions, allowed us to determine the pathlength of aqueous samples with an error below ~50 nm. We implemented this novel approach to analyze interference fringes as a Live Script running in the software Matlab. As an application, we measured absorption spectra of a 97 mM solution of MES buffer (at low and high pH) using cells of various nominal thicknesses (6, 25 and 50 μm). The molar absorption coefficient spectrum for the acidic and basic forms of MES, worked out using pathlengths values determined using the present approach, were virtually identical regardless of the nominal thickness of the cells used, indicating that the thickness determined for the cells were consistent and likely very accurate. These results illustrate the performance of the presented method to determine the pathlength of aqueous samples, as well as for its utility to obtain accurate molar absorption coefficient spectra of water-soluble molecules in the mid-IR region.

Keywords:

Interference fringes, Fourier analysis, sample pathlength, optical constants, FTIR spectroscopy, MES buffer.

1. Introduction

Cells made of two parallel and polished windows separated by a spacer are common when measuring the absorbance of liquid samples by transmission infrared (IR) spectroscopy. Knowledge of the sample pathlength, i.e., the distance that light travels through the sample, allows to determine the molar absorption coefficient spectra of dissolved compounds from their absorption spectra, which can later be used in quantitative analysis. For instance, and among many other potential applications, knowledge of the molar absorption coefficient spectra of the acidic and basic forms of a buffer molecule in the mid-IR region allows to estimate the concentration of its protonated forms and, thus, the pH of a sample from its IR absorption spectrum.[1] This can be accomplished for sample volumes and/or sample conditions not suitable for electrode-based pH measurements, such as hydrated films of proteins.[1] Buffer molecules have been also used as vibrational sensors to detect proton release/uptake events associated to the functional mechanism of proteins.[1–3] Knowing accurately the change in molar absorption coefficient between the acid and basic forms of a buffer can allow, for instance, to quantify the number of released/up-taken protons during the functional mechanism of proteins. As another application, knowledge of molar absorption coefficients can be exploited to determine the concentration of lipids or detergents in a membrane protein sample, a relevant parameter when screening protein crystallization conditions.[4]

In transmission experiments of liquid samples, the pathlength is controlled by the thickness of the cell used to contain the liquid. Knowledge of cell thickness in conjunction with the solute concentration can be used to determine the molar absorption coefficient spectrum of the solute from the experimental absorption spectra by the Lambert-Beer law (after correction for water contributions). However, the accurate determination of the cell thickness is not a trivial task for aqueous samples, mainly because the absorption of liquid water in the mid-IR region makes it necessarily to use very thin cells (5-50 μm). With such thin cells the thickness needs to be determined with nanometric accuracy to keep the relative error in the estimated molar absorption coefficients below 1%. When the cells are *empty* (i.e., filled with air), their thickness can be easily determined from the period of an interference pattern, known as interference fringes, that shows up in absorption spectra.[5] This method is particularly convenient, as it actually measures the pathlength of the light through the sample rather than the cell thickness. Although in ideal conditions both values will be equivalent, the sample pathlength can slightly depart from the cell thickness because of the divergence of the IR beam, the non-parallelism of the cell windows, or because the cell is not perpendicular to the IR beam.[6] While it is important to keep in mind the conceptual difference between the sample pathlength and the cell thickness, we will often use both terms interchangeably in this manuscript whenever we assume ideal measurement conditions.

The period of the interference fringes has been used to determine the thickness of empty cells with nanometric accuracy, but the same has not been accomplished when a cell is filled with an aqueous sample. A practical reason is that the interference fringes reduce notably their intensity when a cell is filled with water and, furthermore, they become hidden under the much stronger background absorbance from liquid water. However, the fundamental problem lays in the fact that the relation between the period of the interference fringes and the cell-thickness becomes wavenumber-dependent in a non-trivial way for absorbing samples (see section 3), with the consequence that decoding the cell thickness from the period of the interferences fringes has not yet achieved to our best knowledge for aqueous samples.

One possible solution to go around the problem of determining the pathlength of aqueous samples is to work with sealed cells. Its thickness can be accurately determined when empty and, once determined, it can be reasonably assumed not to change once they are filled up. However, sealed cells thin enough to study aqueous samples in the mid-IR region are difficult to fill without the formation of air bubbles and they are not easy to clean either, particularly the thinner the cell is. In addition, they are expensive to purchase when compared with dismountable cells. The most economic and versatile dismountable cells are made of just two flat windows plus a thin spacer that determines the cell thickness. A more sophisticated version omits the spacer, and replaces one of the flat windows with a window polished in its central part, with the resulting depression defining the cell thickness.[7] While a dismountable cell is easy to fill and to clean, its thickness significantly changes every time it is dismounted and mounted back.[8] Consequently, one cannot generally assume that the thickness of a dismountable cell remains the same when empty and after being filled with a liquid.

In this contribution we will first review, using Fresnel equations, the nature of the interference fringes in absorption spectra obtained by transmission, deriving analytical expressions to model them. Such characterization will also provide us with some insights regarding the limitations of the Lambert-Beer law caused by light reflection and interference phenomena in transmission measurements, an aspect that has been revisited and review recently in depth.[9–12] Then, we present a novel Fourier-based approach for the analysis of interference fringes in experimental absorption spectra that, in combination with the derived analytical expression for the interference fringes, allows to determine accurately the pathlength of light both for empty cells (filled with air) and for cells filled with aqueous samples. Control experiments with a sealed cell of a nominal thickness of 50 μm filled with liquid H_2O show that a naive Fourier analysis of the interference fringes, i.e., just considering the cell to be filled with a non-absorbing material with a constant refractive index of 1.333, overestimates the pathlength by 1-2 μm (+2% relative error). We traced back most of the source of such systematic error from ignoring the wavenumber dependence of the refractive index of water. When this dependence was accounted for in the analysis, we recovered the sample pathlength with an error below 50 nm (<0.1% relative error). For aqueous solutions, taking a 1 M NaCl solution as an example, we show that to determine the sample pathlength with an error below 50 nm it is sufficient to use the refractive index of the studied aqueous solution in the visible (e.g., 1.345 for 1 M NaCl at 589 nm), approximating its wavenumber-dependent part to that of pure liquid water. We also show that when the refractive index of the studied aqueous solution in the visible is not known, which is expected to be the most habitual case, a variation of the present analysis can provide a straightforward estimation for its value. As a result, the proposed methodology makes it possible to determine the pathlength for virtually any aqueous sample with nanometric accuracy from absorption spectra recorded with an FT-IR spectrometer without the need of any additional equipment.

As a demonstration of the practical utility of the proposed method, we determined the molar absorption coefficient spectrum of the acidic and basic forms of the buffer MES, one of the Good's buffers.[13] Regardless of the thickness of the cell used to measure absorption spectra of MES, the retrieved molar absorption coefficient spectra were almost identical. This result provides a validation for the performance of the present approach to accurately estimate the pathlength of aqueous samples, as well as highlights its utility to determine accurate and reproducible molar absorption coefficient spectra for water-soluble molecules in the mid-IR region.

2. Methods

2.1. Materials. For liquid water we used MilliQ water (MilliQ-Academic, Millipore), with a resistivity of ~20 MΩ cm at 23.8 °C. NaCl and 2-(N-morpholino)ethanesulfonic acid (MES, CAS number 1266615-59-1) were purchased from Sigma-Aldrich (references S7653 and M8250, respectively). For MES buffer solutions, we prepared a 100 mM stock and split it into two (the MES concentration could be slightly lower than 100 mM, as we dissolved 100 mmol of MES per liter of water, ignoring volume changes by the addition of MES). The pH of one of them was adjusted to 3.4 by adding diluted HCl, while the pH of the second one was adjusted to 8.2 by adding diluted NaOH. The volume of added acid and base was registered, and both solutions were brought to the same concentration of MES (97 mM) by adding additional water.

2.2. Data acquisition. Infrared spectra were recorded at 4 cm^{-1} instrumental resolution, using the DTGS detector of a Vertex 80 FTIR spectrometer (Bruker). For the interferometer, we used an optical retardation speed corresponding to a 10 kHz modulation of the built-in HeNe laser. The spectrometer was purged with a dry air generator (Pure gas), with a nominal dew point below −73 °C. We used a sealed CaF_2 cell of a 50 μm nominal thickness (Omni cell, Specac) and a dismountable cell made of two polished 25 mm diameter CaF_2 windows (Korth Kristalle) in combination with mylar spacers (6 μm and 25 μm nominal thickness) and PTFE spacers (100 μm nominal thickness) from Specac. Absorption spectra were measured by placing the cells in a motorized linear stage (Thorlabs, DDSM50/M), automatically alternating 10 scans for the reference and 10 scans for the sample. The process was repeated 10 times, with a total of 100 averaged scans for both the reference and the sample, using an IR beam aperture of 2 mm unless otherwise stated. The temperature of the cell was not controlled, but it was monitored with a temperature sensor (TSP01, Thorlabs), ranging from 25.5 °C to 26.5 °C.

2.3. Determination of the period of the interference fringes, the sample pathlength and the sample pathlength heterogeneity. We wrote a MATLAB Live Script (MATLAB R2022a, MathWorks), freely available at https://www.mathworks.com/matlabcentral/fileexchange/155082-cellthicknessfinder_ftir which implemented the analysis described below.

2.3.1. Determination of the period. The script starts by loading the spectra and selecting the spectral region to be analyzed. If the cell contains an aqueous sample, the script asks for an experimental absorption spectrum of pure water and subtracts it with a factor automatically determined to minimize the residuals (in the least-square sense) in the selected spectral region. Alternatively, the published molar absorption coefficient spectrum of liquid H_2O can be used to generate a synthetic absorption spectrum for subtraction, although this option is not recommended. This step is used to remove contributions from the absorption of water and helps to reveal the underlying interference fringes. The resulting spectrum was baseline corrected before its Fourier transform, with a second order polynomial. For the Fourier transform we applied the Norton-Beer-Medium windowing function to reduce Gibb's oscillations and made 8 levels of zero-filling as an interpolation step, unless otherwise stated. To obtain the magnitude of the Fourier transform, |FT|, we used the MATLAB built-in "fft" function. The period of the interference fringes was determined from the position of the main peak in the |FT| spectrum. This position was estimated by fitting a second order polynomial to the three most intense points of the peak.

2.3.2. Determination of the sample pathlength. As a first approximation, the pathlength of the sample, l, was estimated with Eq. 12, where we used as the period T of the interference fringes the peak

position of its |FT| spectrum. For a more accurate estimate, we simulated the interference fringes with Eq. 9 for empty cells, or using the second term in Eq. 15 for aqueous samples, using the pathlength estimated from Eq. 12 as an initial guess for l. The period obtained after the Fourier analysis of the simulated data was compared with the experimental one, and their discrepancy calculated. The value of l used to constructed synthetic interference fringes was perturbed by 0.01%, and the new discrepancy between the period of the experimental and simulated interference fringes was used to update the value of l to bring this discrepancy to zero. This process was iteratively repeated until we found a value of l for which would generate interference fringes reproducing the experimental period within a discrepancy below 0.001 cm^{-1}. To simulate the interference fringes, we took into account how the refractive index of CaF_2 changes from ~1.43 at 7000 cm^{-1} to ~1.21 at 700 cm^{-1},[14] as collected in https://refractiveindex.info. When working with empty cells, we used the refractive index of air (~1.0003). For liquid H_2O samples we used optical constants of water, $n_{H_2O}(v)$, from Bertie and Lan,[15] available at https://sites.ualberta.ca/~jbertie/JBDownload.HTM#Spectra, and in some cases from Max and Chapados.[16] To the refractive index we subtracted 1.333, the refractive index of water at 589 nm, to obtain the wavenumber-dependent part of the refractive index of water, $\Delta n_{H_2O}(v)$. We divided $\Delta n_{H_2O}(v)$ by 0.967, to correct for a scaling error detected in this work in the molar absorption coefficient spectrum of water published from Bertie and Lan (see Results). We approximated the refractive index of any aqueous solution, *A*, as: $n_A(v) \approx n_A(589\ nm) + \Delta n_{H_2O}(v)$. where $n_A(589\ nm)$ is the refractive index of the considered aqueous solution at 589 nm. We also estimated the pathlength of an aqueous sample from its absorption spectrum, using a modified Lamber-Beer law: $Abs(v) = \varepsilon(v) \times c \times l + b(v)$, where $\varepsilon(v)$ corresponds here to the molar absorption coefficient spectrum from water, taken from Bertie and Lan, c is the molar concentration of H_2O at the working temperature, and $b(v)$ accounts for baseline contributions to the experimental absorbance spectrum (modeled with a first order polynomial). We solved for the value of l minimizing the discrepancy in the least-square sense between the experimental absorption spectrum and $\varepsilon(v) \times c \times l + b(v)$ for a given wavenumber range.

2.3.3. Determination of the heterogeneity in the sample pathlength. We considered the possibility of a heterogeneous sample pathlength, which we described with a Gaussian distribution centered at l and with a full width at half height (FWHH) of Δl. We used Eq. 17 to model the interference fringes in an empty cell and Eq. 18 to model those in aqueous samples. We looked for values of l and Δl bringing the discrepancy between the period of simulated and experimental interference fringes to less than 0.001 cm^{-1}, and which simultaneously best described the band-shape of the peak in the |FT| spectrum in the least-square sense.

3. Theory

Absorbance in a transmission measurement from Fresnel equations. The transmittance, $T(v)$, for a sample (medium 2) placed between two transparent parallel windows (medium 1 and 3) can be determined by Fresnel equations. For simplicity we considered only intensity losses caused by reflection at the window-sample and sample-window interfaces and by the absorbance of the sample, neglecting reflection loses at the initial entrance air-window and final exit window-air interfaces. Under these conditions the transmittance as a function of wavenumber is given by:[6]

$$T(v) = \left| \frac{\hat{t}_{12} \times \hat{t}_{23} \times e^{i\hat{\delta}}}{1 + \hat{r}_{12} \times \hat{r}_{23} \times e^{2i\hat{\delta}}} \right|^2 \qquad (1)$$

where $\hat{t}_{ij}$ and $\hat{r}_{ij}$ are the Fresnel complex amplitude coefficients for the transmitted and reflected radiation between the medium i and the medium j. The Fresnel coefficients differ for radiation polarized parallel (*p*) and perpendicular (*s*) to the plane of incidence. For normal incidence, the conditions considered here, only the *s* component is relevant, and the angle of incidence in the medium i, θ_i, and of refraction in the medium j, θ_j, are zero. Under these circumstances:

$$\hat{t}_{ij} = \frac{2\hat{n}_i cos\theta_i}{\hat{n}_i cos\theta_i + \hat{n}_j cos\theta_j} = \frac{2\hat{n}_i}{\hat{n}_i + \hat{n}_j}; \hat{r}_{ij} = \frac{\hat{n}_i cos\theta_i - \hat{n}_j cos\theta_j}{\hat{n}_i cos\theta_i + \hat{n}_j cos\theta_j} = \frac{\hat{n}_i - \hat{n}_j}{\hat{n}_i + \hat{n}_j} \qquad (2)$$

Thus, at normal incidence the Fresnel coefficients depend only on the complex refractive indices of the medium i ($\hat{n}_i$) and the medium j ($\hat{n}_j$). Note that the complex refractive index of a medium i depends on the wavenumber and it is given by:

$$\hat{n}_i(v) = n_i + ik_i \qquad (3)$$

where n_i and k_i are the optical constants of the medium material, with n_i being the refractive index and k_i the absorption index. Both the refractive and absorption index depend on wavenumber and are related to each other by the Kramer-Kroning transform [17].

On the other hand, the complex exponential components in Eq. 1 account for the absorbance and for the interference of light in the sample, with $\hat{\delta}$ being at normal incidence given by:[6]

$$\hat{\delta} = 2\pi v \times l \times \hat{n}_2 \qquad (4)$$

where l stands for the pathlength of the sample and $\hat{n}_2$ for its complex refractive index.

Before obtaining an analytical expression for the transmittance, we made the reasonable assumption that the two IR windows sandwiching the sample are from the same material, $\hat{n}_1(v) = \hat{n}_3(v)$, and largely transparent in the region of interests, $k_1 \approx 0$. Then, after substituting Eq. 2-4 into Eq. 1 and simplification, we can express the transmittance of light as:

$$T(v) = \frac{A_1}{B_1 10^{\varepsilon_2 \times c \times l} + C_1 sin(4\pi v \times l \times n_2) - D_1 cos(4\pi v \times l \times n_2) + E_1 10^{-\varepsilon_2 \times c \times l}} \qquad (5)$$

where:

$$A_1 = 16n_1^2(n_2^2 + k_2^2); B_1 = (k_2^2 + (n_1 + n_2)^2)^2;$$
$$C_1 = 8k_2 n_1(k_2^2 - n_1^2 + n_2^2)$$
$$D_1 = 2(k_2^4 + 2k_2^2(n_2^2 - 3n_1^2) + (n_1^2 - n_2^2)^2);$$
$$E_1 = k_2^4 + 2k_2^2(n_1 - n_2)^2 + (n_1 - n_2)^4 \qquad (6)$$

The parameter ε_2 in Eq. 5 stands for the wavenumber-dependent molar absorption coefficient used in the Lambert-Beer law, related to the absorption index of the sample k_2 as: $\varepsilon_2 = k_2 \frac{4\pi v}{ln10 \times c}$ where c stands for the sample concentration.

Non absorbing sample. If the cell is filled with a non-absorbing sample, such as air, then $k_2 = 0$ and $\hat{n}_2 = n_2 =$ constant. Under these circumstances Eq. 5 simplifies to:

$$T(v) = \frac{A_2}{(B_2+E_2)-D_2 cos(4\pi v \times l \times n_2)} \qquad (7)$$

where:

$$A_2 = 16n_1^2n_2^2;\ B_2 = (n_1+n_2)^4;\ D_2 = 2(n_1^2-n_2^2)^2;\ E_2 = (n_1-n_2)^4 \qquad (8)$$

The experimental absorbance, $Abs(v)$, will be given by:

$$Abs(v) = log(1/T) = log\left(\frac{B_2+E_2-D_2 cos(4\pi v \times l \times n_2)}{A_2}\right) \qquad (9)$$

We can simplify Eq. 9 using the approximation $log(x) \approx (x-1)/ln10$ to obtain:

$$Abs(v) \approx \frac{B_2+E_2-A_2}{ln10 \times A_2} - \frac{D_2}{ln10 \times A_2} \times cos(4\pi v \times l \times n_2) \qquad (10)$$

For illustration, Fig. 1 shows the calculated absorbance expected for an empty cell with CaF_2 windows and a pathlength of 2 µm, 10 µm, or 50 µm. The results are similar when using the exact Eq. 9 and the approximate Eq. 10, although with some deviations (Fig. 1a). This example also illustrates that the first term in Eq. 10 is a baseline-like feature independent of the cell thickness that arises from light losses by reflection (Fig. 1b), while the second term is oscillatory (with a period depend on the cell thickness) and

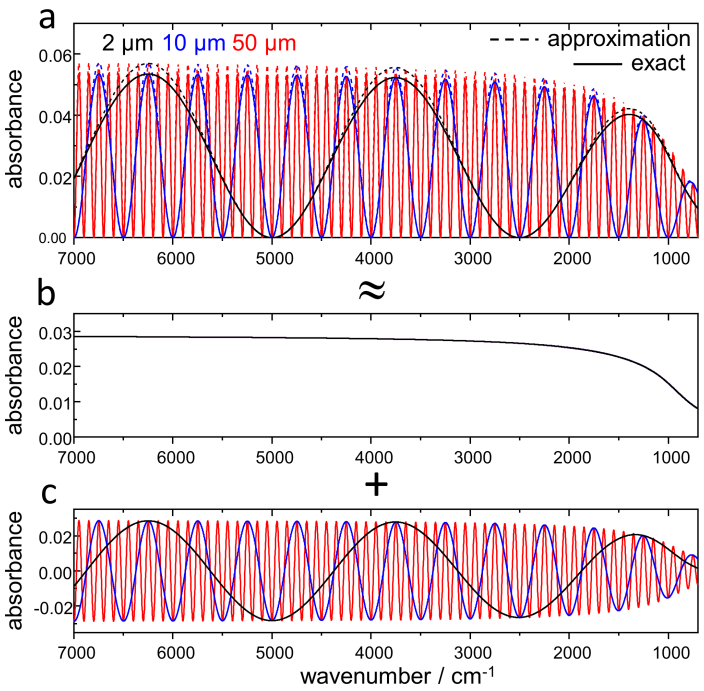

Figure 1. Calculated absorbance in a transmission experiment for an empty cell of various thicknesses (2, 10 or 50 µm) made of CaF_2 windows. (a) Calculated absorbance spectra using either the exact Eq. 9 (derived from Fresnel equations) or the approximated Eq. 10. (b) Calculated baseline-like contribution to the absorbance using the first term of the approximate Eq. 10, independent on the thickness. (c) Calculated oscillatory contribution to the absorbance from the second term of the approximate Eq. 10, dependent on the thickness.

corresponds to light losses by light interference (Fig. 1c).

Because of the cos term in Eq. 9 and Eq. 10, maxima in the transmission and minima in absorption spectra will occur when $4\pi v \times l \times n_2 = \pi N$, ($N = 0, 1, 2, \ldots$), i.e., whenever $2l \times n_2$ is equal to an even number of wavelengths: $2l \times n_2 = \frac{2N}{v} = 2N\lambda$. On the other hand, minima in the transmission and maxima in the absorption spectrum will occur when $4\pi v \times l \times n_2 = \frac{2N+1}{2}\pi$, i.e., whenever $2l \times n_2$ is equal to an odd number of half-wavelengths: $2l \times n_2 = \frac{2N+1}{4v} = \frac{2N+1}{2} \times \frac{\lambda}{2}$. Therefore, the period of the interference fringes , T, not to be confused with the transmittance although we will use the same letter, will be inversely related to the thickness of the sample as:[18]

$$T = \frac{1}{2 \times l \times n_2} \qquad (11)$$

Taking advantage of Eq. 11, the thickness of an empty cell, l, can be estimated from the experimentally determined value of T, as: [8,19]

$$l = \frac{1}{2 \times T \times n_2} \qquad (12)$$

Most commonly in the literature the value of T is calculated from the wavenumber separation Δv between *N* adjacent oscillation maxima, as: [8,19]

$$T = \frac{\Delta v}{N} \qquad (13)$$

Then, after substituting Eq. 13 into Eq. 12 an estimation of the value of l can be obtained from the interference fringes of an absorption spectrum of an empty cell.

Absorbing samples. For an absorbing sample, the absorbance obtained in a transmission measurement will be given by (see Eq. 5):

$$Abs(v) = log(1/T) = log\left(\frac{B_1}{A_1}10^{\varepsilon_2 \times c \times l} + \frac{E_1}{A_1}10^{-\varepsilon_2 \times c \times l} + \frac{C_1 sin(4\pi v \times l \times n_2) - D_1 cos(4\pi v \times l \times n_2)}{A_1}\right) \qquad (14)$$

Rearranging Eq. 14 we can express the experimental absorbance as the conventional Lambert-Beer absorbance, Abs_{LB}, plus a correction term, Abs_{corr}, a correction term that will account for contributions from reflection and interference losses to the experimental absorption spectrum:

$$Abs(v) = Abs_{LB} + Abs_{corr} = \varepsilon_2 \times c \times l + log\left(\frac{B_1 + E_1 \times 10^{-2\varepsilon_2 \times c \times l}}{A_1} + \frac{(C_1 \times sin(4\pi v \times l \times n_2) - D_1 \times cos(4\pi v \times l \times n_2)) \times 10^{-\varepsilon_2 \times c \times l}}{A_1}\right) \qquad (15)$$

Because the correction term in Eq. 15 will be small under most conditions, we can simplify Eq. 15 using the approximation $log(x) \approx (x-1)/ln10$, to obtain:

$$Abs(v) \approx \varepsilon_2 \times c \times l + \frac{B_1 + E_1 \times 10^{-2\varepsilon_2 \times c \times l} - A_1}{ln10 \times A_1} + \frac{(C_1 \times sin(4\pi v \times l \times n_2) - D_1 \times cos(4\pi v \times l \times n_2)) \times 10^{-\varepsilon_2 \times c \times l}}{A_1} \qquad (16)$$

To test how well Eq. 16 works as an approximation for Eq. 15 we simulated the expected absorbance from 7000 to 1000 cm^{-1} for liquid water placed between CaF_2 windows using both equations, assuming sample thickness of 2 µm, 10 µm and 50 µm, and using published optical constants of liquid water.[15]

The agreement between the exact and approximate calculated absorbance was excellent, with a relative error below a 0.4% under all the tested conditions (Fig. S1), validating the approximation in Eq. 16.

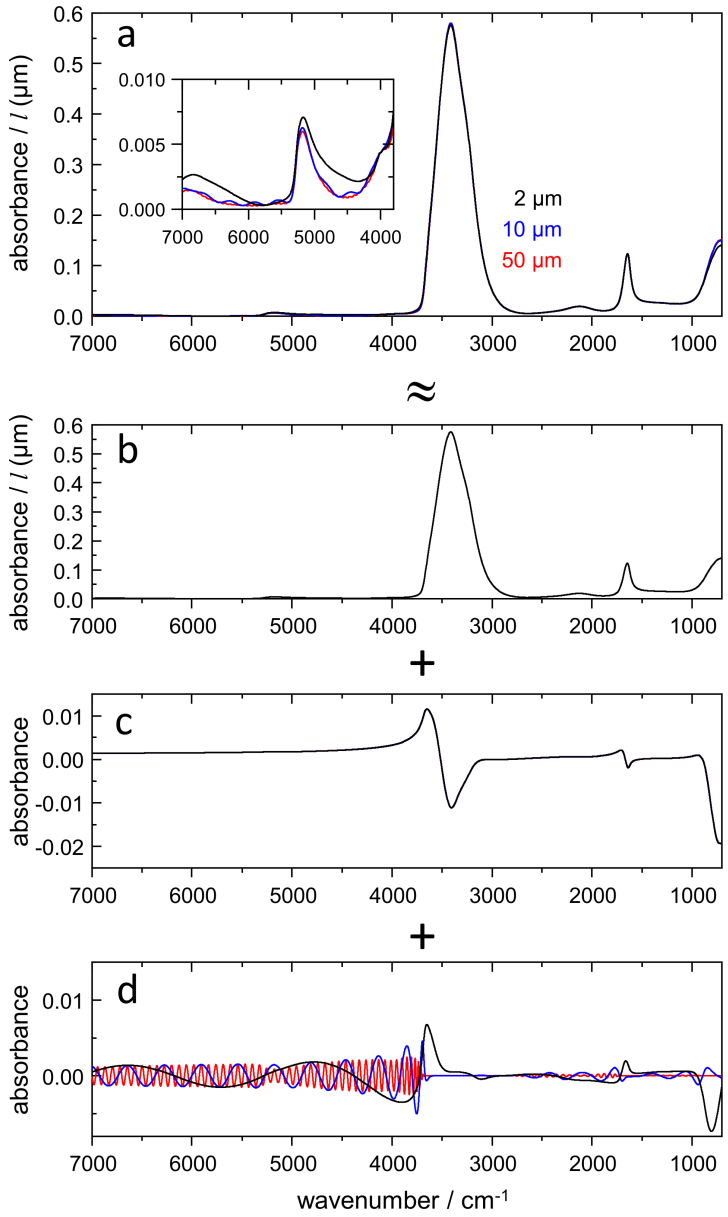

Figure 2. Absorbance from the calculated transmittance of liquid water of various thicknesses (2, 10 or 50 μm) placed between CaF_2 windows. (a) Calculated absorbance spectra using the exact Eq. 15, normalized by the sample thickness l in μm. (Insert) Expanded region of weak absorbance, where distortions by reflection and interference losses become more evident. (b-d) The three terms contributing to the absorbance in a transmission measurement accordingly to the approximated Eq. 16: (b) Lamber-Beer term from sample absorption (1st term in Eq. 16), proportional to the sample pathlength; (c) dispersion-like baseline term from reflection loses (2nd term in Eq. 16), independent of the sample pathlength ; (d) oscillatory term from light interferences (3rd term in Eq. 16), with an oscillation period dependent on the sample pathlength.

One benefit of using the approximate Eq. 16 rather than the exact Eq. 15 is that it allows to disentangle the different contributions present in an absorption spectrum obtained by transmission, as illustrated in Fig. 2 for liquid water. The first term in Eq. 16, the dominant one, is the Lambert-Beer absorbance, the only term with an amplitude directly proportional to the thickness of the sample (Fig. 2b). The other two terms, the second and the third, can be considered distortions that originate from the use of transmission to measure an absorption spectrum. As illustrated in Fig. 2c, the second term in Eq. 16 accounts for a dispersion-like baseline contribution that depends on the optical constants of the sample and the windows. This term is in practice independent of the sample thickness, because $(B_1 - A_1) \gg E_1$. The third term in Eq. 16 is responsible for oscillatory contributions to the absorption spectrum, as illustrated in Fig. 2d. The oscillation period clearly depends on the sample thickness, suggesting that the latter could be inferred from the former, while the amplitude of the oscillations do not change much with the sample thickness. Consequently, the distortions in an absorption spectrum for reflection and interference contributions will be more notable in weakly absorbing regions (see Fig. 2a insert).

Note how the oscillation period of the interferences in Fig. 2d changes with wavenumber, reflecting its dependence on the wavenumber-dependent refractive index of water. Figure 2d also nicely illustrates that for aqueous samples sandwiched between CaF_2 windows the oscillations in an absorption spectrum are largely concentrated above 3700 cm^{-1}, being rather weak in amplitude between 3500-1000 cm^{-1}. Thus, when looking for interference fringes in experimental absorption spectra from aqueous samples we should place our focus in the spectral region above 3700 cm^{-1}.

4. Results

4.1. Determining the pathlength of empty cells by a Fourier transform analysis of the interference fringes.

As an example of how the analysis of the interference fringes allows to estimate the pathlength of empty cells, Fig. 3b shows the experimental absorbance measured by transmission of a sealed cell made of CaF_2 with a nominal thickness of 50 μm, placed perpendicular to the IR beam. Besides the absorbance from the CaF_2 windows, apparent below 1300 cm^{-1}, and the positive absorbance offset caused by intensity loses due to light reflections at the CaF_2/air interfaces, the absorbance shows an oscillatory pattern often referred to as interference fringes. These oscillations arise from the interference at the detector of the direct IR beam and the IR beam reflected at the two internal CaF_2/air interfaces (red and green light paths in Fig. 3a). Counting the distance between 25 of such maxima in Fig. 3b, we could estimate an average period of the interference fringes to be 96.96 cm^{-1}. Applying this period to Eq. 12, and considering that $n_2 \approx 1.0003$ for air at room-temperature, we determined a cell thickness of 51.55 μm.

A more convenient (and robust) way to determine the period of the interference fringes is by means of a Fourier analysis.[5,20] We restricted this analysis to the 7000-1400 cm^{-1} spectral region, skipping the absorption from the CaF_2 windows. For practical reasons, the truncated spectrum was baseline corrected (Fig. 3c, gray trace) and multiplied by a windowing function (Fig. 3c, black trace) before performing the FT. One of the weakness noted before for the Fourier analysis of interference fringes was the relatively large spacing between data points after the FT, which limited the accuracy by which

the period of oscillations could be determined.[21] To reduce this data spacing we performed 8-levels of zero-filling prior to the FT, as done before.[5,20]

Figure 3d plots the resulting magnitude of the Fourier transform, |FT|: the magnitude of the oscillations as a function of their period in cm^{-1}. One intense peak appears, which corresponds to the main period of the interferences. To recover the thickness of the cell with nanometric precision we need to determine the period of the interference fringes with three decimal places. However, even after 8-levels of zero-filling, the separation of the points around the peak maximum in the |FT| spectrum was still of ~0.15

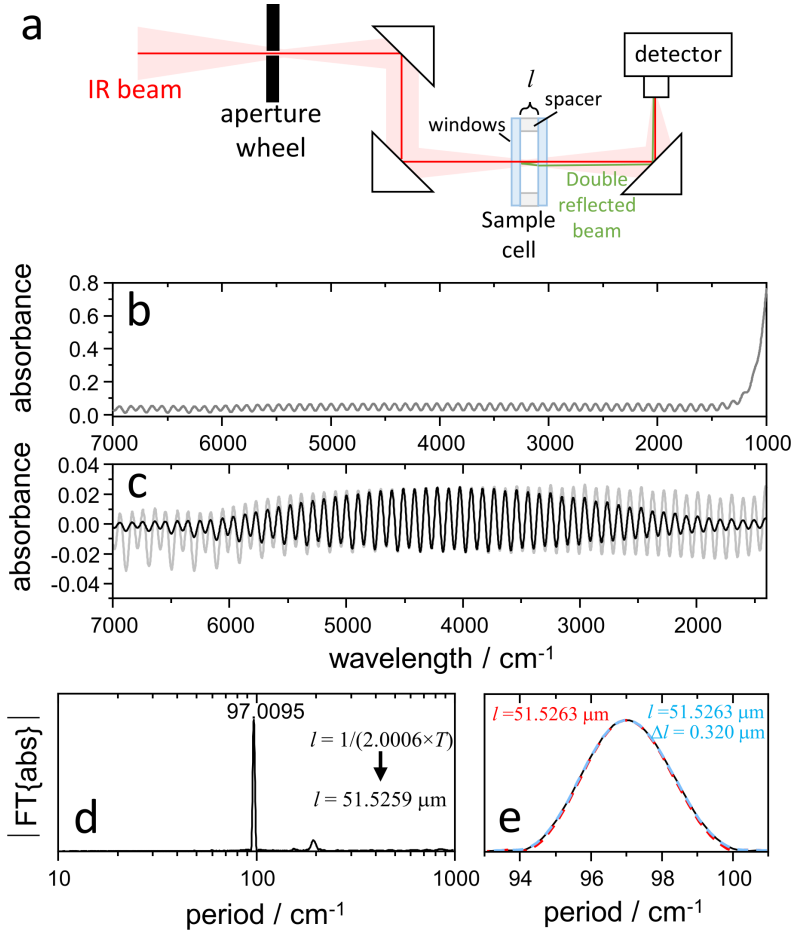

Figure 3. Analysis of the interference fringes of an empty sealed cell with a nominal thickness of 50 µm. (a) Scheme, showing the sample cell, the path of the IR beam (in red), the pathlength of light in the cell, l, and the double reflected beam (in green), including an aperture that controls the beam divergence. (b) Experimental absorption spectrum of an empty sealed CaF_2 cell from 7000 to 1000 cm^{-1}, obtained with an IR beam aperture of 2 mm. (c) Absorption spectrum from 7000 to 1400 cm^{-1} offset to zero (gray), and after applying a windowing function (Norton-Beer-Medium) to reduce signal leakage after the Fourier transform (black). (d) Magnitude of the Fourier transform of the spectrum in back in (c), represented as a function of the period (in logarithmic scale). (e) Same as (d), but the period is represented from 93 to 101 cm^{-1} (solid black trace). In (d) the pathlength l was estimated from the period of the peak using Eq. 12 (left), and in (e) by fitting the peak period using Eq. 9 as a model of the interference fringes (red dashed trace). The heterogeneity in the pathlength, Δl, was estimated in (e) by fitting the peak period with Eq. 17 as a model of the interference fringes (blue dashed trace). In all cases we used 1.0003 as the refractive index of the air filling the cell.

cm^{-1} (Fig. S2, see inset), too large for our purposes. The peak maximum was determined by fitting a second order polynomial to the three more intense points of the peak in the |FT| spectrum (Fig. S2, inset), providing a result of 97.0095 cm^{-1}. Applying Eq. 12, we inferred from the period a thickness for the empty cell of l = 51.5259 μm.

The first question we asked ourselves was how precise our estimation for the thickness of the empty cell was, i.e., how much this estimate could vary from measurement to measurement. For that, we measured every ~200 s an absorption spectrum, for a total of ~164 min. The estimated thickness from the Fourier analysis of the interference fringes changed from spectrum to spectrum (Fig. S3 blue trace), with a standard deviation of 1.6 nm. However, the estimated thickness clearly drifted with time, suggesting that part of the variation might originate from actual changes in the cell thickness, probably from small drifts in the temperature of the cell. To obtain a more robust estimate of the error, e.g., less sensitive to temperature drifts, we calculated differences in thickness estimates between consecutive measurements (Fig. S3, red trace). The standard deviation for thicknesses differences between consecutive measurements was 0.4 nm, which we consider a reasonable estimate for the precision of the present method for empty cells under our measuring conditions.

Once we conceived a methodology to obtain the thickness of empty cells with sub-nanometric precision, we asked ourselves about its accuracy. Although we lack appropriate standards to experimentally determine it, we might expect it to be potentially sub-nanometric given the sub-nanometric wavelength accuracy of the He-Ne laser that controls the movement of the interferometer in a FTIR spectrometer. However, we found that the value estimated for the period and, thus for the cell thickness, depends on how the data was pre-processed before FT (baseline correction polynomial order, windowing function used, or level of zero-filling), leading to variations in the estimated thickness that could be close to $\pm$ 1 nm. Even more severe was the dependence of the estimated cell-thickness on the spectral range analyzed: 51.5259 μm when using the 7000-1400 cm^{-1} spectral range, but 4 nm larger for 7000-4000 cm^{-1} and 2 nm shorter for 4400-1400 cm^{-1}. This latter effect could be due from light of different wavenumber experiencing a slightly variations in their pathlength travelled within the cell. Considering the above variability, the accuracy in the thickness determined for empty cells is probably limited by the analysis, in the order of some few nanometers.

Aiming to go beyond the limitations of obtaining the cell thickness from the period of the oscillations by means of Eq. 12, we explored a different strategy. Briefly, we constructed a synthetic absorption spectrum modeled using Eq. 9, which we pre-processed prior to FT in the same way the experimental spectra was. The parameter l of the synthetic spectrum was optimized until its peak period after FT exactly matched the one determined from the experimental spectrum. Although we expected this new approach to determine the sample thickness to be much less affected by how an absorption spectrum was preprocessed or cut prior to FT, this was only the case when applied to synthetic absorption spectra recreated with Eq. 9. When analyzing interference fringes from experimental absorption spectrum, the estimated thickness was still dependent on how spectra were pre-processes prior to FT and, particularly, on which spectral segment was analyzed. Nevertheless, this newly introduced approach to estimate the sample pathlength from the interference fringes has some clear benefits, and will be essential when working with aqueous samples, as we will see.

We applied this newly introduced approach to analyze the interference fringes in Fig. 3c. A value of $l =$ 51.5263 μm was needed to generate with Eq. 9 interference fringes with a period of 97.0095 cm^{-1} (Fig.

3e), which corrects by 0.4 nm the thickness estimated by directly feeding the period of the oscillations into Eq.12 (Fig. 3d). Repeating the analysis on four consecutive measurements we obtained $l = 51.5267 \pm 0.0003$ μm (mean plus/minus one standard deviation).

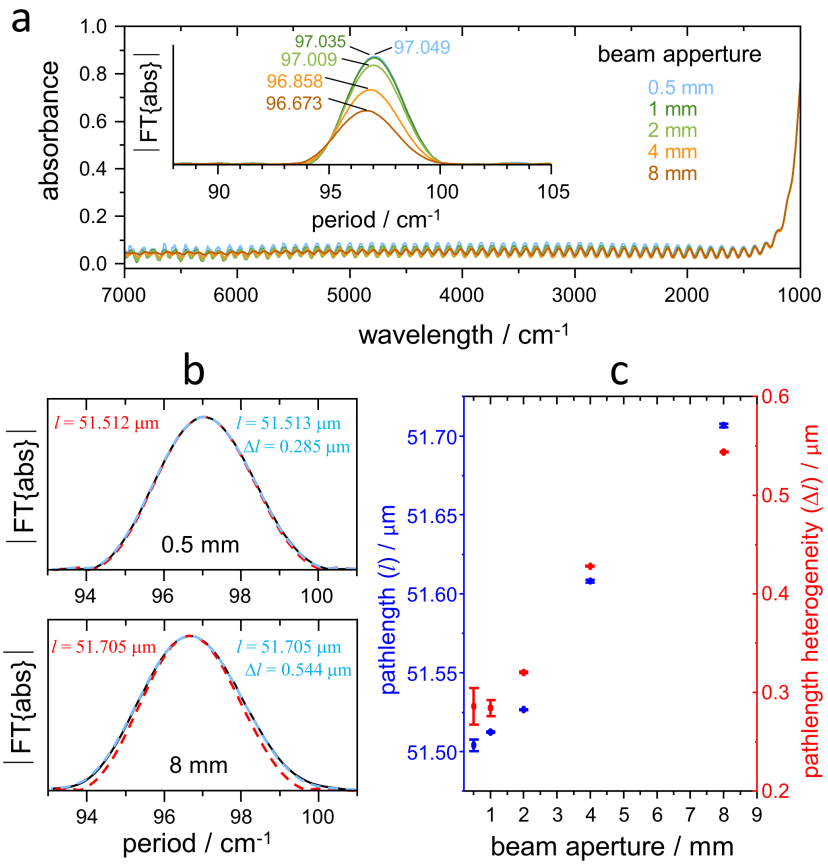

Figure 4. Analysis of the interference fringes of an empty sealed cell of 50 μm nominal thickness as a function of the IR beam aperture used. (a) Experimental absorption spectrum from 7000 to 1000 cm^{-1} for IR beam apertures ranging from 0.5 mm to 8 mm. The insert shows the magnitude of the FT of the spectra from 7000 to 1400 cm^{-1}. (b) Magnitude of the period from 93 to 101 cm^{-1} for two extreme apertures, (top) 0.5 mm and (bottom) 8 mm (black traces), together with a fit using either interference fringes created with Eq. 12, that ignores pathlength heterogeneities (red dashed traces), or interference fringes created with Eq. 17, that account for pathlength heterogeneities (blue dashed traces). (c) Estimated sample pathlength and sample pathlength heterogeneity as a function of the IR beam aperture used.

We noted that the |FT| of the simulated interference fringes (Fig. 3e red dashed trace) did not only match the experimental peak period (black trace), but also described very well its band-shape. The agreement was not perfect though, as the peak for the simulated data was slightly narrower than for the experimental one (compare black and red traces in Fig. 3e). A similar observation has been reported before and has been interpreted to originate from heterogeneities in the pathlength, caused either by heterogeneities in the cell thickness (e.g., deviations of the two windows from planarity), as well as by an angle of incidence of the IR beam departing from 0° due to its conic shape (beam divergence).[6,20] In our case, we opted for simplicity to model the interference fringes as originating from a pathlength

distributed as a Gaussian function. Because the FT of a Gaussian is also a Gaussian, we modified *ad hoc* Eq. 9 to include heterogeneity in the sample pathlength:

$$Abs(v) = log\left(\frac{B_2+E_2-D_2cos(4\pi v\times l\times n_2)\times exp\left(-\frac{\pi^2}{ln2}\left(\frac{4\times v\times \Delta l\times n_2}{10^4}\right)^2\right)}{A_2}\right) \qquad (17)$$

where Δl is the full width at half height (FWHH) of the Gaussian distribution assumed for the sample pathlength. Optimizing the center ($l = 51.5263$ μm) and the FWHH ($\Delta l = 0.3199$ μm) of the Gaussian distribution we could excellently model with Eq. 17 both the peak position and band-shape of the |FT| of the experimental spectrum (Fig. 3e, blue dashed trace). Repeating the analysis on four consecutive measurements we obtained $l = 51.5267 \pm 0.0003$ μm and $\Delta l = 0.3204 \pm 0.0010$ μm (mean plus/minus standard deviation).

The absorption spectrum in Fig. 3b was obtained using an IR beam aperture of 2 mm. Figure 4 shows similar results but obtained using both smaller and larger IR beam apertures. The first observation is a reduction of the intensity of the interference fringes as the aperture increases, particularly at high wavenumbers. In addition, the period of the fringes slightly shifts with increasing aperture, and the peak after |FT| also gets broader (Fig. 4a, inset). These changes can be rationalized after considering that the larger the beam aperture the more divergent the IR beam and the larger area of the cell covered by the IR beam. If the two windows of the cell are not perfectly parallel to each other, the "effective" cell thickness will depend on the probed area.[6,20] Even if the cell windows are perfectly parallel, the fact that the IR beam is not perfectly collimated will make the pathlength (i.e., the traveled distance of light inside the cell) to increase with the aperture. In the present example, the "average" pathlength increased by ~200 nm when increasing the IR beam aperture from 0.5 mm to 8 mm (Fig. 4c, blue points). For the same two reasons mentioned above, the pathlength becomes also more broadly distributed the higher the beam aperture used, a feature reflected in a faster decay of the interference fringes with the wavenumber and in the increased broadness of the peak in the |FT| of the absorption spectrum (Fig. 4a). When modeling the sample pathlength heterogeneity as a Gaussian function, its FWHH increased from ~0.29 μm to ~0.54 μm as the IR beam aperture increased from 0.5 mm to 8 mm (Fig. 4b, blue dashed traces, and Fig. 4c, red points).

We also explored the reproducibility of the thickness determined for an empty sealed cell with respect to its physical manipulation. This will be particularly important for the following sections dealing with aqueous samples, where the cell needs to be removed from the sample compartment and placed back after being filled with the aqueous solution to be studied. To test the reproducibility of the estimated cell thickness to respect its physical manipulation, we repeatedly introduced the empty cell in the sample compartment of the FTIR, measure and absorption spectrum, removed the empty cell from the FT-IR sample compartment of the FTIR spectrometer, filled it up with water, gently emptied the cell blowing pressurized air, and put the empty cell back at the same position in the FTIR sample compartment. The estimated thickness of the cell changed by 5 ± 3 nm in each manipulation (n = 7). This variation is mostly ascribable, in our opinion, to sub-millimeter errors when repositioning the cell back into the sample compartment. This conclusion is supported by the fact that the interference fringes (Fig. 5a), their period (Fig. 5b) and the estimated cell thickness (Fig. 5c) change smoothly as the cell is translated in a direction perpendicular to the IR beam. A translation-dependent thickness (Fig. 5c) indicates that the sealed cell we used is slightly wedged. Given the slope of the cell thickness *versus* the

translation of the cell, a variation of ± 5 nm in the cell thickness could be explained by an error of approximately ± 50 μm when repositioning the cell in the sample compartment, a reasonable error considering that this was done manually.

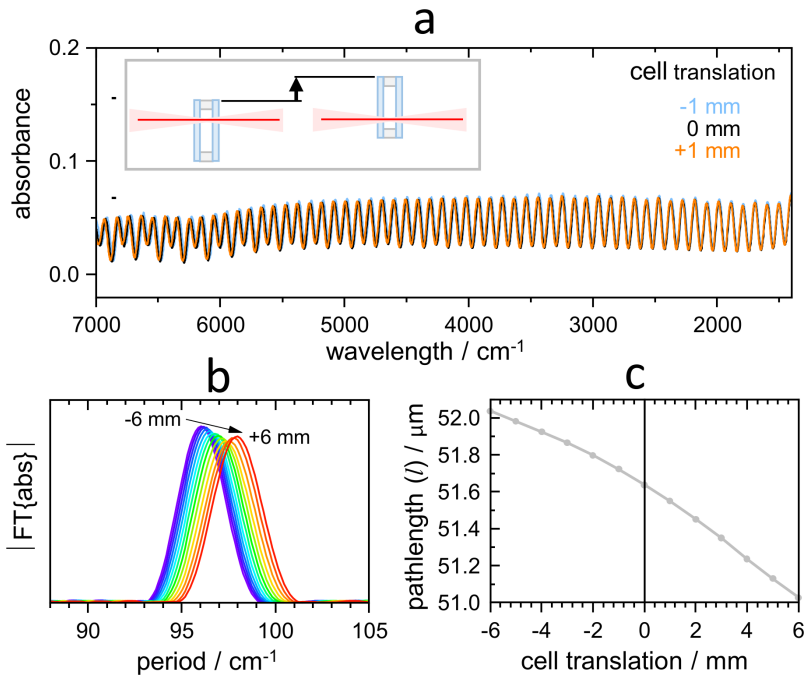

Figure 5. Analysis of the interference fringes of an empty sealed cell of 50 μm nominal thickness as a function of the translation of the cell perpendicular to the IR beam. (a) Experimental absorption spectrum of an empty sealed cell from 7000 to 1400 cm^{-1} (IR beam aperture of 2 mm) at three different cell translation distances. The insert illustrates how the cell was translated. (b) Magnitude of the FT of the interference fringes for different translations. (e) Estimated sample pathlength as a function of the translation of the cell.

4.2. Determining the pathlength of a water-filled cell using the Lambert-Beer law.

We filled the sealed cell with liquid H_2O and measured nine absorption spectra, with a time difference between the first and last spectrum of two hours. First, it was necessary to confirm which was the actual cell thickness at the spot sampled by the IR beam. To this end we also measured several absorption spectra of the sealed cell when empty, before adding the liquid water and after removing it. From the resulting spectra, analyzed from 7000 to 3900 cm^{-1} to be consistent with how spectra from the water-filled are analyzed later, we estimated a cell thickness of 51.5896 ± 0.0003 μm and a heterogeneity of 0.3542 ± 0.0020 μm before filling the cell with water and of 51.5784 ± 0.0016 μm and o0.346 ± 0.006 μm after removing the water from the cell at the end of the experiment. Thus, we expect a thickness of the cell when filled with liquid water to lay in between the above values, i.e., a thickness of around 51.584 ± 0.007 μm and a heterogeneity of around 0.350 ± 0.006 μm.

The average absorption spectrum of the cell filled with water is presented in Fig. 6a. The interference fringes are barely visible, with an intensity notably reduced because the similar refractive indices of H_2O (~1.333) and of the CaF_2 windows (~1.4). On the other hand, the remaining oscillations in the absorption

spectra become visually hidden under the much intense water absorption bands (Fig. 6a). Likely due to these difficulties, the weak interference fringes in aqueous solutions have never been used, to our knowledge, to estimate sample pathlengths.

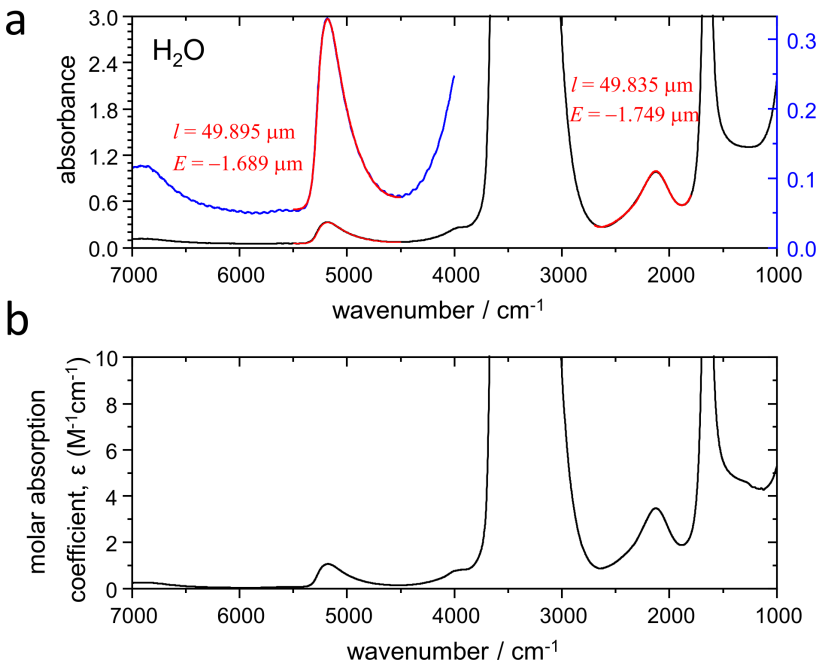

Figure 6. Determination of the sample pathlength of a sealed cell of 50 μm nominal thickness filled with liquid water (H_2O) using Lambert-Beer law. (a) Absorption of the sealed cell (actual thickness determined to be of 51.584 ± 0.007 μm when empty) filled with liquid water (black trace). The region between 7000 and 4300 cm^{-1} is expanded, helping the visualization of small interference fringes present (blue trace). The regions between 7000-4300 cm^{-1} and 2800-1900 cm^{-1} are fitted using the molar absorption coefficient spectrum of water in (b) (red traces). The sample thickness estimated by applying the Lambert-Beer law, and the error made, are indicated. (b) Molar absorption spectrum of water used for the Lambert-Beer law, reproducing data from Bertie and Lan [15].

The pathlength of a cell filled with liquid water can be estimated from its absorption spectrum, using the Lambert-Beer law. When using the absorption coefficient of liquid water from Bertie and Lan, [15] reproduced in Fig. 6b, and the concentration of water molecules at the working temperature (55.34 M), we arrived to a sample pathlength of 49.895 ± 0.013 μm (mean and std of the mean from nine spectra) to best reproduce the absorbance in the 5500-4000 cm^{-1} region (red trace in Fig. 6a). When trying to match the 2800-1800 cm^{-1} spectral region (red trace in Fig. 6a) the estimated pathlength was quite similar: 49.835 ± 0.031 μm. Despite their consistency, these two estimates are systematically lower by ~1.7 μm than the pathlength determined for the empty sealed cell, i.e., a ~3.3% relative error. Therefore, we concluded that the molar absorption coefficient spectrum of liquid H_2O from Bertie and Lan[15] is slightly overestimated, at least in the 5500-4000 cm^{-1} and 2800-1800 cm^{-1} regions, and should be rescaled by ~0.967 for best predicting the sample pathlength. After this correction the sample pathlength was estimated to be 51.598 ± 0.014 μm (5500-4000 cm^{-1} region) and 51.536 ± 0.032 μm (2800-1800 cm^{-1} region), with an error of +14 ± 16 nm and -48 ± 33 nm, respectively. The need of rescaling by 0.967 of the molar absorption coefficient spectrum of Bertie and Lan is reasonable considering the uncertainty of 4-6% reported for the 5500-4000 cm^{-1} and 2800-1800 cm^{-1} regions.[15]

Better estimated were obtained when using the molar absorption coefficient spectrum of liquid H_2O from5500-4000 cm^{-1} of Max and Chapados,[16] which we needed only to rescale by 0.995 to recover the pathlength estimated when the cell was empty.

This example illustrates the problem of relying solely on molar absorption coefficient spectra and Lambert-Beer law to determine the sample pathlength and highlights the importance of having alternative methods. We will also see later, taking a 1 M NaCl solution as an example, that the use of the molar absorption coefficient of liquid water, even when correctly rescaled, can fail to accurately provide the pathlength of aqueous solutions because of changes in absorption bands from water in the presence solutes.

4.3. Determining the pathlength of a water-filled cell by a Fourier transform analysis of the interference fringes. The only region where some interference fringes are visually apparent in the absorption spectrum of water is above ~3800 cm^{-1} (Fig. 6a, insert). To better observe and analyze these oscillations, we first need to subtract the contribution of water absorbance to the experimental absorption spectra. Following Eq. 15, this could be done by subtracting the expected Lambert-Beer absorbance calculated with the molar absorption coefficient data of water from Bertie and Lan[15], but the subtraction was not fully satisfactory in revealing the interference fringes free from water contributions (Fig. S4, blue trace). Much worse results were obtained when using the molar absorption coefficient data of water from Max and Chapados [16] for the subtraction (Fig. S4 light blue trace). Instead, noticing that non-Lambert-Beer contributions to the experimental absorption spectrum are expected to get proportionally smaller the thicker the sample is (see Fig. 2a), we used an absorption spectrum of liquid water measured the same day with a much thicker cell (Fig. 7a, gray trace). The subtraction nicely revealed the underlaying interference fringes (see Fig. 7a orange trace, and Fig. S4 red trace). The |FT| of the interference fringes from 7000 to 3900 cm^{-1} is presented in Fig. 7c. The most intense peak is located at 70.725 $\pm$ 0.030 cm^{-1}, accompanied by some nearby peaks (Fig. 7c, right panel, black trace). The peak from the interference fringes coming from the 125 μm thick sample used in the subtraction was expected at around 28 cm^{-1} but was not observable above the noise level.

Taking the refractive index of water to be constant and equal to 1.333, the one determined in the visible, we arrived to $l = 53.035 \pm 0.023$ μm when applying Eq. 12. This value overestimates by 1.451 μm the value of l determined for the empty cell (relative error of 2.8%). We might suspect that this error arises because the refractive index of water in the 7000-3900 cm^{-1} range is not 1.333 but centered instead at around 1.29 (see Fig. 7b). However, when using the latter value in Eq. 12 the sample pathlength was even more overestimated. Instead, the overestimation of the sample thickness when using Eq. 12 mostly originates from the fact that refractive index of water is not constant but increases with the wavenumber in the analyzed spectral range. To accurately estimate the sample pathlength, we simulated the interference fringes with the second term of Eq. 15, using corrected optical constants of liquid H_2O from Bertie and Lan,[15] reproduced in Fig. 7b for the refractive index. Then, we optimized the value of l until the |FT| of the spectra simulated with the second term of Eq. 15 displayed a peak period matching the experimental one (Fig.7c, right panel, red dashed trace). The best agreement was obtained for l = 51.643 $\pm$ 0.022 μm, which is only +59 $\pm$ 23 nm off from the thickness determined when the sealed cell was empty (see Section 4.1). This notable improvement in accuracy illustrates the need to consider the dependence with the wavenumber of the refractive index of the sample.

A further improvement was obtained when acknowledging for potentially heterogeneities in the sample pathlength, modeled as a Gaussian, using an *ad hoc* modification of the second term of Eq. 15:

$$Abs_{corr}(\nu) = log\left(\frac{B_1+E_1\times10^{-2\varepsilon_2\times c\times l}}{A_1} + \frac{\left(C_1\times sin(4\pi\nu\times l\times n_2)-D_1\times cos(4\pi\nu\times l\times n_2)\right)\times exp\left(-\frac{\pi^2}{ln2}\left(\frac{4\times\nu\times\Delta l\times n_2}{10^4}\right)^2\right)\times10^{-\varepsilon_2\times c\times l}}{A_1}\right) \quad \text{(Eq. 18)}$$

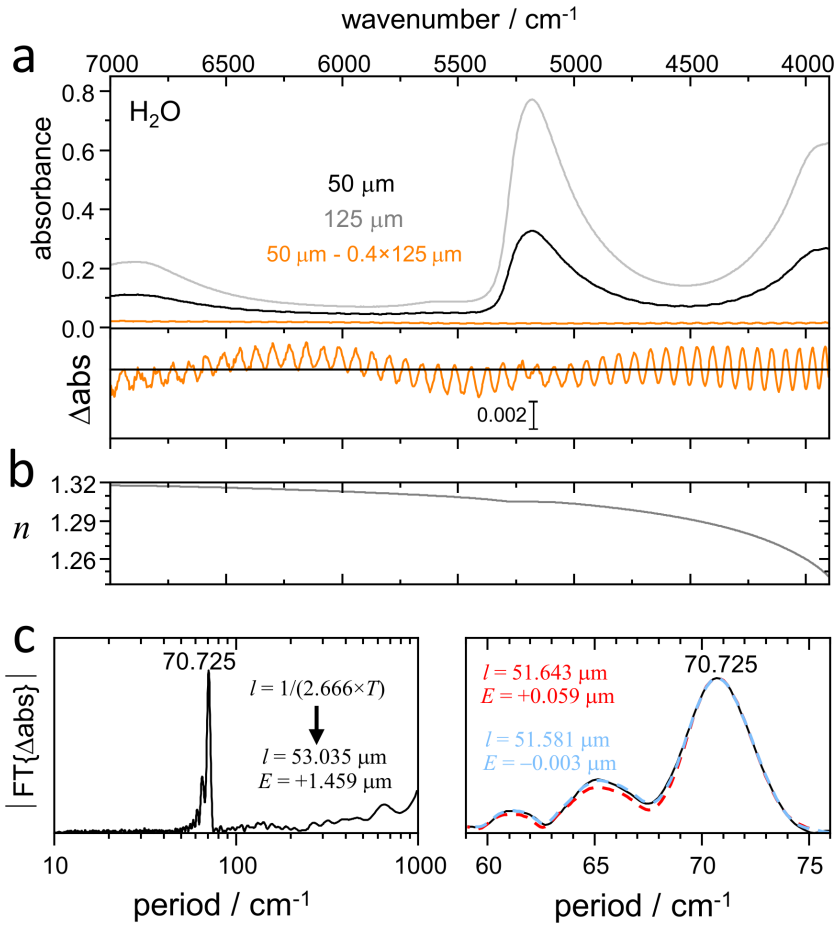

Figure 7. (a, top) Experimental absorption spectrum of the sealed cell filled with water, with an actual thickness determined to be of 51.584 ± 0.007 μm when empty (black trace), and absorption spectrum of a dismountable cell with a thickness of ~125 μm filled with water (gray trace). (a, bottom) Difference spectrum to cancel water absorption contributions of the sealed cell between 7000-3900 cm^{-1}, revealing the interference fringes (orange trace). (b) Corrected refractive index of liquid water from 7000 to 3900 cm^{-1} from Bertie and Lan[15]. (c) Magnitude of the Fourier transform of the difference spectrum in (a) as a function of the period, from 10 to 1000 cm^{-1} in logarithmic scale (left) and from 59 to 76 cm^{-1} in a linear scale (right, black traces). In (c, left) the period of the main peak is indicated, together with the pathlength estimated using Eq. 12 (with $n_2 = 1.333$), and its error. In (c, right) the peak was fitted using either the second term of Eq. 15 as a model (red dashed trace) or Eq. 18 (blue dashed trace), using the refractive index spectrum of pure water in (b), and the estimated pathlength (and error) is given in red and in blue, respectively.

The best agreement between the model and the experimental data was obtained for l = 51.581 $\pm$ 0.024 μm, which is only -3 $\pm$ 25 nm off from the thickness determined when the sealed cell was empty. Finally, the estimated thickness heterogeneity was 0.248 $\pm$ 0.027 μm, significantly below the value estimated for the empty cell: 0.350 $\pm$ 0.007 μm. The smaller pathlength heterogeneity when the cell is filled with could be due to the IR beam becoming more collimated when the cell is filled with water by a lensing effect.

To discard that the excellent results in estimating the thickness of a cell filled with water by analysis of the interference fringes could be ascribable to chance, we repeated the same experiment on two different days. The error made between the pathlength estimated for the cell filled with water and for the empty cell was of +69 $\pm$ 30 nm and +82 $\pm$ 22 nm when ignoring heterogeneities, and of +15 $\pm$ 35 nm and -36 $\pm$ 22 nm when these were considered in the analysis, confirming the excellent results.

4.4. Effect of uncertainties in the refractive index of the aqueous medium on the estimated pathlength. Our analysis to estimate the pathlength of aqueous (H_2O-based) samples with nanometric precision relays on using information about the refractive index of liquid water. This refractive index, $n_{H_2O}(v)$, can be separated, for convenience, in a constant component, $n_{H_2O}(589\,nm) = 1.333$, plus a wavenumber dependent component, $\Delta n_{H_2O}(v)$, such that $\Delta n_{H_2O}(v) = n_{H_2O}(v) - 1.333$. Because $\Delta n_{H_2O}(v)$ is related to the absorption index of water, $k_{H_2O}(v)$, by the Krames-Köning transform, and $k_{H_2O}(v)$ is in turn directly related to the molar absorption coefficient of water, $\varepsilon_{H_2O}(v)$, $n_{H_2O}(v)$ is susceptible to uncertainties as much as $\varepsilon_{H_2O}(v)$ is. To explore the potential impact of this source of error, we repeated the analysis in Section 4.3., but making $\Delta n_{H_2O}(v)$ 5% larger or 5% smaller. While a 5% error in $\varepsilon_{H_2O}(v)$ leads to a 5% error in the estimated sample pathlength when using the Lambert-Beer law, our simulations show that a 5% error in $\Delta n_{H_2O}(v)$ only changes the estimated sample pathlength by a 0.1% when analyzing the interference fringes with the presented methodology. This makes our proposed method to estimate the pathlength of aqueous samples relatively robust to uncertainties (or changes) in the wavenumber-dependent part of the refractive index.

On the other hand, our method is also sensitive to errors in the constant part of the refractive index: our test show that a 5% relative error in $n_{H_2O}(589\,nm)$ leads to a 5% relative error in the estimated sample pathlength. Fortunately, the refractive index of water at 589 nm is accurately known. Moreover, it does not vary much with the temperature, decreasing less than 0.00015 per each degree we depart from 295 K. Consequently, small changes in the ambient temperature can be ignored with a minor cost in accuracy. More critical is the effect of solutes on the refractive index of water. For instance, Tan and Huang have reported the refractive index for three electrolyte solutions (NaCl, KCl, and $CaCl_2$), a polar solution (glucose solution), a nonpolar solution (ethyl acetate solution), and a protein solution (bovine serum albumin solution) in water.[22] For the first five solutions, the refractive index at 589 nm increased with respect to that of pure water by less than 0.0034 (less than a ~0.25%) for solute concentrations up to 0.1 M. In the case of proteins, taking BSA as a reference, the refractive index of water was reported to increase by just 0.004 (~0.3%) when using a concentration as high as 10 mg/ml. Thus, in the above commented cases, the increase in refractive index can be ignored at the cost of overestimating the sample pathlength by less than 0.25%-0.3%. For highly concentrated solutions, as

illustrated in the next section for a 1 M NaCl solution, considering the actual refractive index at 589 nm might be important for an accurate estimation of the sample pathlength.

4.5 Determining the pathlength of a cell filled with a highly concentrated aqueous solution by a Fourier transform analysis of the interference fringes. After removing the water sample from the sealed cell, we filled it with a ~1 M NaCl solution (0.06 g NaCl /g total, i.e., 6 % in weight) and measured four absorption spectra. The cell was then cleaned, and its absorption spectrum measured again when empty. From the absorption spectra of the empty cell obtained before and after the 1M NaCl measurement, we estimated a cell thickness of 51.576 $\pm$ 0.003 μm and a heterogeneity of 0.349 $\pm$ 0.009 μm.

The average absorption spectrum of 1 M NaCl between 7000 and 3900 cm^{-1} is presented in Fig. 8a (black trace), together with a spectrum of 1 M NaCl measured using a dismountable cell with a thickness of ~90 μm (gray trace). The subtraction between the two spectra (with an appropriate factor) reveals the interference fringes from the sealed cell (Fig. 8a bottom, orange trace). Figure 8c shows the |FT| of the interference fringes between 7000 and 3900 cm^{-1}, with the main peak corresponding to an oscillation period of 70.29 $\pm$ 0.05 cm^{-1} (left panel). This period is significantly smaller than the one corresponding to the cell filled with pure water, 70.725 $\pm$ 0.030 cm^{-1} (see Fig. 7c, left panel). Using Eq. 12 and taking a refractive index of 1.333 we arrive to an estimate of l = 53.364 $\pm$ 0.035 μm, which is off from the expected value by +1.79 μm. The refractive index of NaCl in water at 589 nm has been measured for concentrations ranging from 0.5% in weight (~0.086 M) to 26% in weight (~ 5.3 M),[23] being 1.343 for 6% in weight (~1 M). Using this latter value, we arrived to l = 52.969 $\pm$ 0.035 μm, which is still off by +1.39 μm from the expected pathlength (Fig. 8c, left panel).

As explained in previous sections, to estimate accurately the sample pathlength from the period of the interference fringes we need to model them with Eq. 15 (or Eq. 18), which requires the refractive index of the aqueous sample solution as a function of the wavenumber. The refractive index of the sample can be separated as the sum of a fixed part and a wavenumber-dependent part. For the variable part, we just took that of pure H_2O from Bertie and Lan with an already commented scaling correction, and for the constant part we used the value of 1.343 determined for a 1 M NaCl solution at 589 nm.[23] Using this approximation (shown in Fig. 8b) we estimated from the period of the interference fringes a sample pathlength of 51.589 $\pm$ 0.035 μm, which is off by just +13 $\pm$ 35 nm from the thickness estimated when the cell was empty (Fig. 8c, right panel, read dashed trace). When accounting the heterogeneities in the pathlength the thickness was estimated to be 51.528 $\pm$ 0.030 μm, off by -48 $\pm$ 30 nm, and the FWHH was estimated to be 0.25$\pm$ 0.03 nm (Fig. 8c, right panel, blue dashed trace). We repeated the same experiment one additional time on a different day. The sample pathlength was recovered with an error of +22 $\pm$ 18 nm to respect the estimation when the sealed cell was empty, and when the pathlength heterogeneity was considered in the analysis the error was -40 $\pm$ 26 nm, which is both cases are exceptionally low.

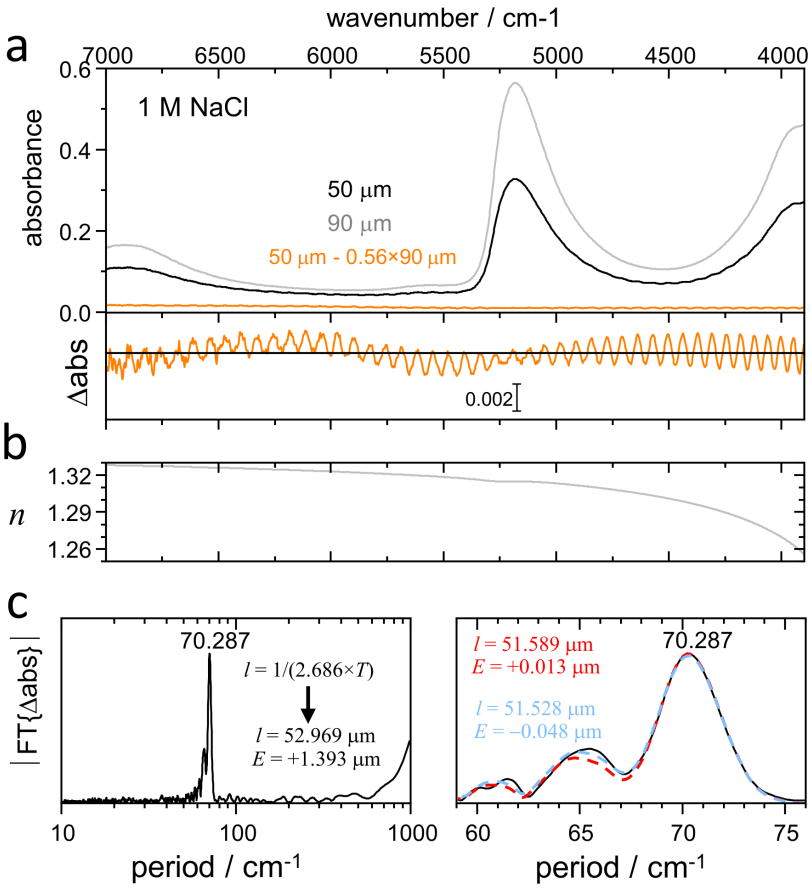

Figure 8. Analysis of the interference fringes to estimate the sample pathlength of a sealed cell of 50 μm nominal thickness filled with a 1 M NaCl aqueous solution. (a, top) Experimental absorption spectrum of the sealed cell filled with 1 M NaCl, with an actual thickness determined to be of 51.576 ± 0.003 μm when empty (black trace), and absorption spectrum of 1 M NaCl in a dismountable cell with a thickness of ~90 μm (gray trace). (a, bottom) Difference spectrum to cancel the water absorption of the sealed cell between 7000-3900 cm^{-1}, revealing the interference fringes (orange trace). (b) Approximate refractive index of 1 M NaCl, constructed from the refractive index of liquid water upshifted by 0.011, the difference between the refractive index of 1 M NaCl (1.344) and water (1.333) at 589 nm. (c) Magnitude of the Fourier transform of the difference spectrum in (a) as a function of the period, from 10 to 1000 cm^{-1} in logarithmic scale (left) and from 59 to 76 cm^{-1} in a linear scale (right, black traces). In (c, left) the period of the main peak is indicated, together with the pathlength estimated using Eq. 12 (with $n_2 = 1.344$), and its error. In (c, right) the peak was fitted using either the second term of Eq. 15 as a model (red dashed trace) or Eq. 18 (blue dashed trace), using the approximate refractive index of 1 M NaCl in (b), and the estimated pathlength (and error) are given in red and in blue, respectively.

When estimating the sample pathlength from Lambert-Beer law, using the molar absorption coefficient of liquid water of Bertie and Lan in the 5500-4000 cm^{-1} and 2800-1800 cm^{-1} regions, the error made was -1.3 μm and -3 μm, respectively, and +0.44 μm and +1.3 μm when using a rescaling of 0.967. When using the molar absorption coefficient of liquid water of Max and Chapados in the 5500-4000 cm^{-1} and 2800-1800 cm^{-1} regions the error was +0.13 μm and -1.6 μm, respectively, and of +0.38 μm and -1.4 μm

when using a rescaling of 0.995. The error, quite large, indicates that the molar absorption coefficient of water cannot approximate well-enough the absorption of water in the presence of salt.

We should note our strategy to determine the pathlength of aqueous samples from the period of the interference fringes might start to fail at solute concentrations when the change of its refractive index with wavenumber is no longer sufficiently well approximated by that of pure water, and. As an extreme example we studied a saturated solution of NaCl (26.3 wt%, or ~5.3 M), with a reported refractive index at 589 nm of 1.380.[23] In these experiments, conducted on a different day, the sample pathlength of the cell was estimated to be 51.6742 $\pm$ 0.0020 μm when empty. We estimated a pathlength of 51.53 $\pm$ 0.13 μm when potential heterogeneities in the pathlength were ignored. The uncertainty in sample pathlength estimate was particularly high in these experiments because the amplitude of the interference fringes was quite weak, possibly because the reflective index of the sample being now closer to that of the CaF_2 windows. The error made in the estimated pathlength was ~-150 $\pm$ 130 nm when ignoring heterogeneities and, when these were considered, of ~-220 $\pm$ 140 nm. In spite these "large" errors, the relative error in determining the pathlength was still below a ~0.4%, which should still be acceptable in most applications.

4.6. Determining the value of the refractive index of an aqueous solution from the interference fringes. In one example used in the previous section, a 1 M NaCl aqueous solution, we could accurately estimate the sample pathlength from the period of the interference fringes because we knew the value of the refractive index of this solution at 589 nm from the literature. However, values for the refractive index are not available for most aqueous solutions and, when available, they are not provided at all concentrations, which seems a serious shortcoming for the general applicability of the present method. Thus, in this section we provide a simple strategy to infer the value of the refractive index of an aqueous solution at 589 nm from the period of the interference fringes in the 7000-3900 cm^{-1} range. We just need to measure interference fringes from the aqueous solution of interest and of pure water, both measured using the same sealed cell of fixed thickness, measured at the same spot (to ensure the same pathlength). Then, we divide the period determined for the oscillations in the H_2O sample and in the aqueous solution of interest, multiplying the result by the refractive index of water at 589 nm, 1.333. As an example, when applied to 1 M NaCl we determined the refractive index to be: 70.725 / 70.287 × 1.333 ≈ 1.341. When repeated in an independent experiment the result was: 70.400 / 69.857 × 1.333 ≈ 1.343. The estimated refractive index, 1.342 $\pm$ 0.0015, is in reasonably good agreement with the value reported in the literature for the refractive index of 1 M NaCl, 1.344.[23] Because this simple approach tacitly assumes that the variable part of the refractive index does not differ between the aqueous solution of interest and pure water, it will start to fail for highly concentrated solutions. For instance, when applied to a saturated NaCl solution, we estimated a refractive index of 1.373 at 589 nm, while the reported experimental value is 1.380.[23]

4.7. Application to determine molar absorption coefficient spectra of the buffer MES in two protonation states. MES is a Good's buffer with a pK_a of 6.15 at 25 ^oC. [24] Figure 9a shows the molecular structures of the acidic and basic forms. To determine the molar absorption coefficient of these two forms we prepared aqueous solutions of 97 mM, at pH 8.2 and pH 3.4. These two solutions were measured in a dismountable cell using mylar spacers with a nominal thickness of 6 μm and 25 μm, and with the sealed cell used in the previous sections (nominal thickness of 50 μm). The resulting absorption spectra for the 6 μm and 50 μm-thick cell, dominated by the absorption from water, are

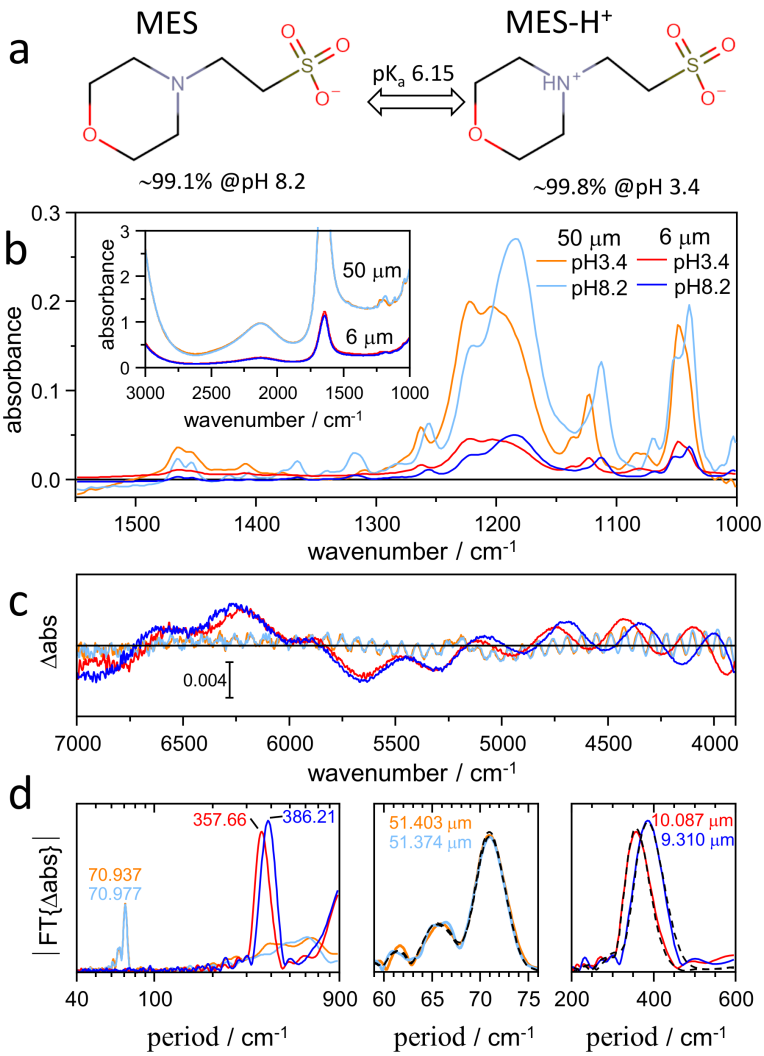

Figure 9. Analysis of interference fringes to estimate the sample pathlength of 97 mM aqueous solutions of acidic and basic forms of the buffer MES recorded in cells of 6 and 50 μm nominal thickness. (a) Molecular structure of the basic and acidic forms of the buffer MES, indicating their expected proportion of each represented species at pH 8.2 (99.1% of the basic form) and at pH 3.4 (99.8% of the acidic form). (b) Absorption of MES at 97 mM recorded at two pH values, after subtraction of water absorbance measured in a cell of the same thickness. The inset shows the absorbance prior to the subtraction of the water contribution. (c) Subtraction of the water absorption in spectra of MES in the 7000-4200 cm^{-1} region using a spectrum of pure water recorded with a thicker cell, revealing the interference fringes (color-coded as in (b)). (d) Magnitude of the Fourier transform of spectra of the interference fringes in (c) as a function of the period (color-coded as in (b)), represented from 40 to 900 cm^{-1} in logarithmic scale (left). Expanded region from 59 to 76 cm^{-1} with the period peak from the 50 μm-thick cell (middle) and from 200 to 600 cm^{-1} with the period peak of the 6 μm-thick cell (right). The expanded regions (middle and right panels) include a fitting using Eq. 18 as a model for the interference fringes (dashed black traces). The estimated sample pathlength is indicated in each case.

displayed in the inset of Fig. 9b (data from the 25 μm-thick cell is omitted for clarity). After subtracting the water contribution, using absorption spectra of pure water measured in cells with the same nominal thicknesses, we isolated the absorption contributions from MES (Fig. 9b).

To determine the actual pathlength of the samples we applied the protocol developed in previous sections: we subtracted a water spectrum measured with a thicker cell to reveal the interference fringes in the 7000-3900 cm^{-1} region (Fig. 9c), and then performed the FT. Note the different strategy when the goal was to remove the contribution of water to reveal the absorbance of the buffer MES (water spectrum measured with a cell of a thickness as similar as possible to that of the sample), and when the goal was to reveal the interference fringes as unaltered as possible (water spectrum measured with a thicker cell). The |FT| spectra from the revealed interference fringes provides us with the period of the oscillations: around 370 cm^{-1} for the samples measured with a 6 μm spacer (Fig. 8d, left panel), around 130 cm^{-1} for the samples measured with a 25 μm spacer (not shown), and around 71 cm^{-1} for the sealed cell of 50 μm nominal thickness (Fig. 8d, left panel). From these periods, we estimated pathlengths modeling the interference fringes with Eq. 18, optimizing the parameter l (and Δl) until we reproduced the period from the experimental spectra, as explained in detail in previous sections. This analysis requires as an input the refractive index of the MES solutions at 589 nm. Because of its low concentration (below 100 mM) the value corresponding to pure water in the visible (1.333) is already a reasonably good approximation. Nevertheless, we estimated the refractive index of the MES solutions as explained in section 4.6: we compared the period of the oscillations in a sealed cell, first filled with pure water and then with 97 mM MES solutions. From the ratio of their periods, we arrived at a refractive index of 1.3354 for the acidic form of MES and of 1.3349 for the basic form of MES, i.e., ~1.335. With this value, we constructed an approximated refractive index spectrum for 97 mM MES as: $n_{MES}(v) \approx 1.335 + \Delta n_{\mathrm{H_2O}}(v)$.

Modeling the peaks in the |FT| spectra we estimated a sample pathlength when using the 6 μm spacer of 10.087 μm and 9.310 μm for MES at pH 3.4 and 8.4, respectively, and of 51.403 μm and 51.374 μm, respectively, when using the sealed cell (see Fig. 9d, middle and right panels). For the cell with a 25 μm spacer, the estimated thicknesses were 27.731 μm and 28.187 μm for samples at pH 3.4 and 8.4, respectively (not shown).

From the absorption spectra of MES (Fig. 9b), its concentration (97 mM), and the estimated sample pathlengths, we determined the molar absorption coefficient spectra of the acid and basic forms of MES from 1550 to 1000 cm^{-1} (Fig. S5). We accounted for the fact that spectra measured at low and high pH contain minor fractions from the basic and acidic forms of MES, according to its pK_a and the Henderson-Hasselbalch equation. The molar absorption coefficient spectra are presented in Fig. 10a and Fig. 10b after a baseline correction with a first order polynomial. Notice how, despite using samples of quite different nominal thicknesses and, thus, with very different absorbance, we arrived at very consistent estimates of molar absorption coefficient spectra for the acidic and basic forms of MES, with a standard deviation of ~4.5 M^{-1} cm^{-1} for the acidic and ~2.5 M^{-1} cm^{-1} for the basic form. The discrepancies between the estimated molar absorption coefficient spectra from the different cells are largely ascribable to baseline errors, and when using the 50 μm-thick cell to the high absorbance of the sample, which reaches 2 at 1000 cm^{-1}. To better compare the estimated molar absorption coefficient spectra obtained from different cells Figure S6 shows their second derivative, a spectral processing that minimizes baseline contributions. There it can be appreciated the excellent agreement between molar absorption coefficients determined from cells of different thicknesses, which validate our analysis to determine the pathlength of aqueous solutions.

Figure 10c shows, from 3000 to 1000 cm^{-1}, the estimated changes in the molar absorption coefficient of MES upon its protonation. The agreement in the 1550-1100 cm^{-1} region is excellent for all the different cell thicknesses used. The agreement between 3000 and 2400 cm^{-1} is somehow lower, yet still reasonably good. In the 2300-1550 cm^{-1} we have some notable discrepancies, which can be mostly ascribed to interference fringes present in the measurements with the 6 μm and 25 μm cell but with a negligible intensity for the 50 μm cell. At other spectral regions, particularly below 1550 cm^{-1}, the interference fringes are apparently absent even when using the 6 μm spacer, likely due to the strong attenuation of the double reflected beam by the strong background absorbance of water (see inset in Fig. 9b).

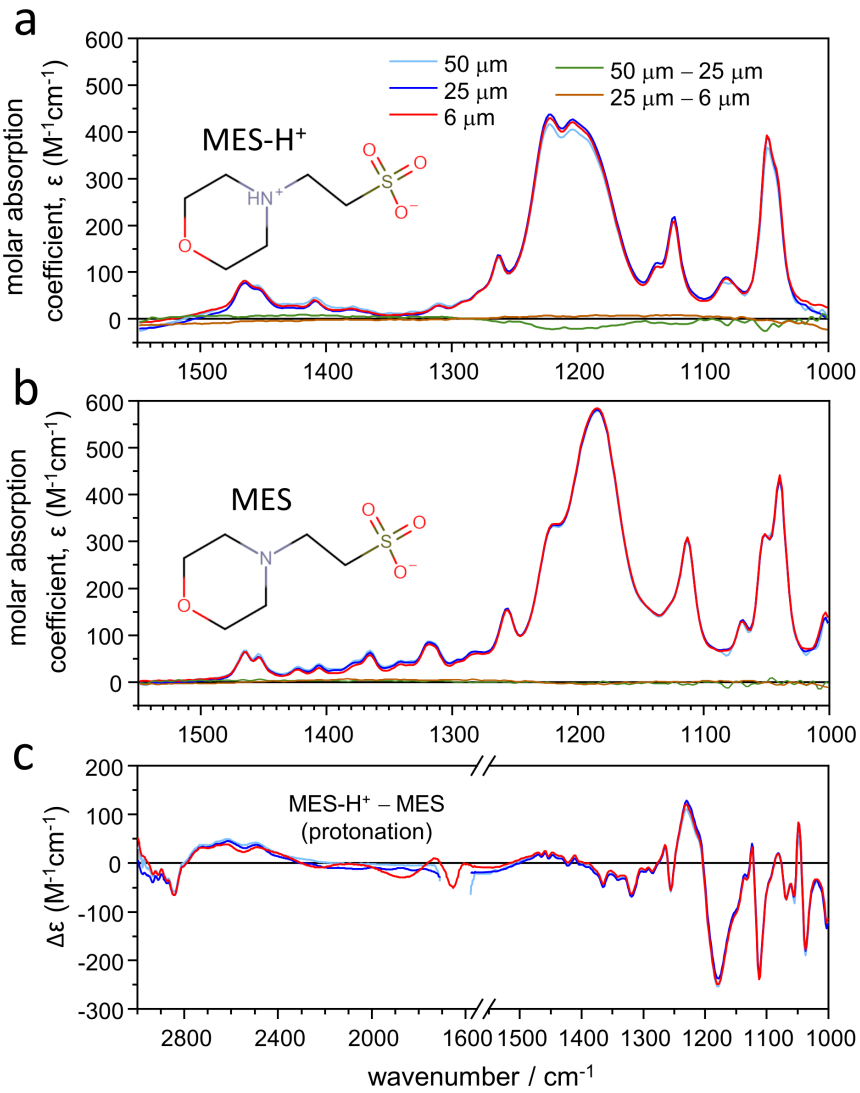

Figure 10. Baseline-corrected estimation of molar absorption coefficient spectra of MES from absorption spectra recorded in cells with nominal thicknesses of 50, 25 and 6 μm. (a) Molar absorption coefficient spectra for the acidic form of MES calculated from samples of different thicknesses, and their discrepancy. (b) Same as (a), but for the basic form of MES. (c) Difference molar absorption spectra between the acidic and basic forms of MES, representing MES protonation (color-coded as in (a)).

Finally, we compared the here determined molar absorption coefficient spectrum of the acidic and basic forms of MES with those determined before by attenuated total reflection (ATR), using a diamond crystal.[1] In the case of the ATR experiments, obtaining molar absorption coefficient spectra requires determining the effective pathlength as a function of wavenumber. That was experimentally done by comparing the absorption spectrum of liquid water measured by ATR with the Lambert-Beer absorption spectrum expected for a 1 μm thick sample of liquid water, the latter calculated with the molar absorption spectrum of water determined by Bertie and Lan [15] and the concentration of H_2O in liquid water. Then, we assumed the same effective pathlength for an aqueous solution of MES, ignoring potential changes in the effective penetration by the presence of MES. As shown in Fig. S5, the agreement between the molar absorption spectra of MES estimated here by transmission and previously by ATR is reasonably good, although with clear notable discrepancies that can be largely assigned to errors when estimating the effective pathlength in ATR measurements.

4.8. The effect of cell tilting on the sample pathlength. Tilting the cell is a common strategy to reduce the intensity of the interference fringes. As an example, Fig. 11 shows the interference fringes when using a 50 μm-thick empty sealed cell of CaF_2, tilted by ~20°. The amplitude of the oscillations is reduced by a factor of ~8 compared with a measurement at a 0° tilt (compare Fig. 11 and Fig. 3b). However, a Fourier analysis of the interference fringes (Fig. 11, Inset) reveals that the reduced amplitude of the interference fringes goes together with a notable increase in the inhomogeneity of the period and, thus, presumably also of the pathlength of light within the cell. The |FT| spectrum shows an asymmetric peak, with a maximum at a period of 97.710 cm^{-1} and shoulders at 99.5 and 102.9 cm^{-1}. Although a future expansion of Eq. 9 to apply for angles of incidence other than 0° might be needed for a correct interpretation of this observation, such asymmetric peak might indicate the coexistence of three light

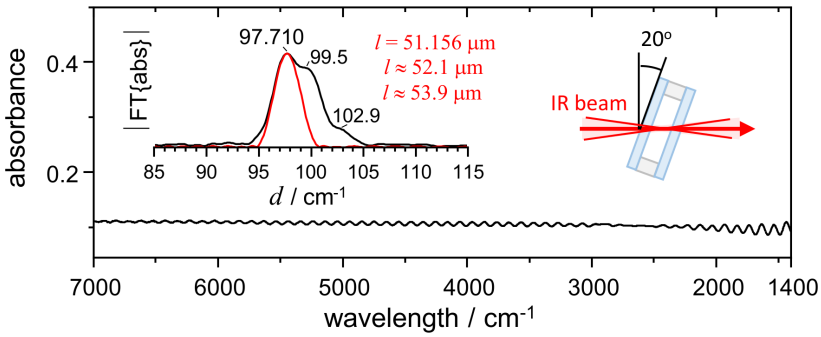

Figure 11. Interference fringes for an empty sealed cell with a nominal thickness of 50 μm, tilted by 20°. The inset displays the magnitude of the Fourier transform (black), together with the simulated data assuming a pathlength of 51.156 μm. Note that the experimental data is much broader and with shoulders, indicating that there is not a single well-defined pathlength but either multiple discrete pathlengths or asymmetrically distributed pathlengths.

paths inside the cell, of lengths ~51.2, ~52.1 and ~53.9 μm, or more reasonably an asymmetric continuous distribution of pathlengths. This situation could arise because when the IR beam is not perfectly collimated it enters the cell at variable angles, experiencing slightly different pathlengths, a feature that can be enhanced for tilted samples. Thus, although titling the sample can be a useful option to reduce interference fringes, considering our observation we recommend avoiding or at least minimize the tilting of cells in studies requiring well-defined sample pathlengths, such as in the determination of molar absorption coefficient spectra.

5. General discussion

We have presented a Fourier-based analysis of the period of the interference fringes that allows determining the pathlength of light through aqueous samples, with an error below ~50 nm. After recording an absorption spectrum from the sample using an FT-IR spectrometer, the analysis involves: 1) the subtraction of the background absorption from water to reveal more clearly the interference fringes in the sample spectrum; 2) calculating the magnitude FT spectrum from the interference fringes; 3) identification of the main peak in the magnitude FT spectrum and determination of its period; 4) estimation of the sample pathlength by creating synthetic interference fringes that reproduces the period of the main peak in the magnitude FT. This last step requires knowledge about the refractive index spectrum of the aqueous sample in the studied range. For diluted solutions, the refractive index spectrum of the sample can be approximated to that of pure water, with good results. When such an approximation is not suitable, or to obtain more accurate results, a better yet still simple approximation is to use the fixed part of the refractive index of the studied aqueous solution in combination with the wavenumber-dependent part of the refractive index of pure water. We show that this latter approximation, despite its simplicity, works excellently well for solutions with moderate to high concentrations of solutes (e.g., a 1 M NaCl solution), although starts to be less accurate for very highly concentrated solutions (e.g., a saturated NaCl solution).

Some attention should be paid to the subtraction of the background absorption of water, which is essential to reveal the hidden interference fringes. The spectrum used for the subtraction needs to be recorded with a cell of a different thickness, preferable thicker. The reason is that the residual of this subtraction will combine the interference fringes from both spectra, whose period can be disentangled by the FT only if they differ sufficiently. In addition, using a thicker cell allows for subtraction factors smaller than 1, reducing the relative intensity of the interference fringes from the subtracting spectrum and, thus, better revealing the interference fringes from the spectrum of interest.

We should point out that the methodology presented here has some limitations that can challenge its applicability. One is that, for best results, it requires knowledge of the refractive index of the studied aqueous sample at a reference wavelength, e.g., at 589 nm. This information is available for some but not for all aqueous solutions. However, we have shown that the refractive index of an aqueous solution at a reference wavelength can be inferred by using a sealed cell of fixed thickness and comparing the period of the interference fringes of the studied solution and of pure liquid water. Thanks to this simple trick, the presented approach is potentially able to determine the pathlength for virtually any aqueous solution.

One technical limitation when estimating the pathlength of aqueous samples from interference fringes is the need of recording spectra extending to wavenumbers as high as possible, e.g., to 7000 cm^{-1}. The reason is that, in aqueous solutions, the interference fringes are only clearly observable above 3900 cm^{-1}, and enough oscillations need to be recorded for a better determination of their period. FTIR spectrometers with interferometers that are not well aligned show a decay of their intensity above 4000 cm^{-1},[19] which can prevent reliably measuring absorbance spectra extending to wavenumbers as high as 7000 cm^{-1}. Another technical limitation is that the sample cell needs to be perpendicular to the IR beam. Tilting the sample reduces the intensity of the interference fringes, making it more difficult to

detect their period, and it also seems to introduce asymmetric heterogeneities in the sample pathlength, up to that point that talking about a single pathlength may become meaningless.

Regarding the range of applicability of the Fourier-based analysis presented here, the larger pathlength that can be determined is physically limited by the instrumental resolution. At 4 cm^{-1} spectral resolution, the smaller period that can be measured is around ~4 cm^{-1}, which for empty cells corresponds to a pathlength of ~1.25 mm. Although not shown here, we have been able to determine easily pathlengths of ~1 mm, much larger than needed for aqueous solutions. On the other hand, the smaller pathlength that we can reliably determine is limited by the mixing of the interference fringes with baseline error and residuals from imperfect water subtraction. These two last contributions lead to background signals with large periods in the |FT| spectrum. Consequently, it can be quite challenging to determine the sample pathlength when the period of the interference fringes is larger than ~800 cm^{-1}. This sets the approximate lower limit for the applicability of the present approach to aqueous solution with a pathlength >5 μm. To determine thinner pathlengths one might need to do a similar analysis as done here but on visible spectra, where the period of interference fringes from sub-micrometer thin samples can be more clearly determined. [25]

6. Summary

We have developed, tested, and validated a novel strategy to determine the pathlength of aqueous samples from the analysis of the interference fringes. This new methodology is accurate and will significantly improve the estimation of molar absorption coefficient spectra of water-soluble molecules in the mid infrared region, including biological buffers and relevant biomolecules. We deployed a Matlab Live Script that implements the described methodology.

CRediT authorship contribution statement

Mónica Gutierrez-Salazar: Formal analysis; Investigation. **Victor A Lorenz-Fonfria:** Conceptualization; Software; Formal analysis; Investigation; Writing - review & editing.

Funding

This work was supported by grants projects BFU2017-91559-EXP and PID2019-106103GB-I00 founded by MCIN/AEI/ 10.13039/501100011033, a predoctoral fellowship BES-2017-080385 founded by MCIN/AEI/ 10.13039/501100011033 and by "ESF Investing in your future", and an Excellence Unit "María de Maeztu" grant CEX2019-000919-M founded by MCIN/AEI/ 10.13039/501100011033.

Data and code availability

All data presented in the figures of this paper are available at Mendeley Data [DOI: 10.17632/cyf3zxmksz.1]. The Matlab Live Script implementing the analysis of the interference fringes is available at Matlab File Exchange [https://es.mathworks.com/matlabcentral/fileexchange/155082-cellthicknessfinder_ftir].

Supplementary material

Supplementary Figures S1 to S7.

References

[1] V.A. Lorenz-Fonfria, M. Saita, T. Lazarova, R. Schlesinger, J. Heberle, pH-sensitive vibrational probe reveals a cytoplasmic protonated cluster in bacteriorhodopsin., Proc. Natl. Acad. Sci. U. S. A. 114 (2017) E10909–E10918. https://doi.org/10.1073/pnas.1707993114.

[2] F. Baymann, D.E. Robertson, P.L. Dutton, W. Mäntele, Electrochemical and Spectroscopic Investigations of the Cytochrome bc_1 Complex from *Rhodobacter capsulatus*, Biochemistry. 38 (1999) 13188–13199. https://doi.org/10.1021/bi990565b.

[3] H. Suzuki, M. Sugiura, T. Noguchi, Monitoring Proton Release during Photosynthetic Water Oxidation in Photosystem II by Means of Isotope-Edited Infrared Spectroscopy, J. Am. Chem. Soc. 131 (2009) 7849–7857. https://doi.org/10.1021/ja901696m.

[4] C.J.B. daCosta, J.E. Baenziger, E. John, A rapid method for assessing lipid:protein and detergent:protein ratios in membrane-protein crystallization, Acta Crystallogr. Sect. D Biol. Crystallogr. 59 (2002) 77–83. https://doi.org/10.1107/S0907444902019236.

[5] H.M. Heise, Comparison of different algorithms for the interferometric determination of thicknesses in the µm-range by IR-spectroscopy, Fresenius. J. Anal. Chem. 346 (1993) 604–607. https://doi.org/10.1007/BF00321253.

[6] J.P. Hawranek, P. Neelakantan, R.P. Young, R.N. Jones, The control of errors in i.r. spectrophotometry-III. Transmission measurements using thin cells, Spectrochim. Acta Part A Mol. Spectrosc. 32 (1976) 85–98. https://doi.org/10.1016/0584-8539(76)80055-4.

[7] S.Y. Venyaminov, F.G. Prendergast, Water (H_2O and D_2O) Molar Absorptivity in the 1000–4000 cm^{-1} Range and Quantitative Infrared Spectroscopy of Aqueous Solutions, Anal. Biochem. 248 (1997) 234–245. https://doi.org/10.1006/abio.1997.2136.

[8] G.E. Tranter, FTIR spectroscopy of aqueous solutions, in: Encycl. Spectrosc. Spectrom., Elsevier, 2016: pp. 762–769. https://doi.org/10.1016/B978-0-12-409547-2.12157-2.

[9] T.G. Mayerhöfer, S. Pahlow, J. Popp, The Bouguer-Beer-Lambert Law: Shining Light on the Obscure, ChemPhysChem. 21 (2020) 2029–2046. https://doi.org/10.1002/CPHC.202000464.

[10] T.G. Mayerhöfer, H. Mutschke, J. Popp, Employing Theories Far beyond Their Limits-The Case of the (Boguer-) Beer-Lambert Law, ChemPhysChem. 17 (2016) 1948–1955. https://doi.org/10.1002/cphc.201600114.

[11] T.G. Mayerhöfer, H. Mutschke, J. Popp, The Electric Field Standing Wave Effect in Infrared Transmission Spectroscopy, ChemPhysChem. 18 (2017) 2916–2923. https://doi.org/10.1002/CPHC.201700688.

[12] J.J. Max, C. Chapados, Infrared transmission equations in a five media system: Gas and liquid, J. Math. Chem. 47 (2010) 590–625. https://doi.org/10.1007/S10910-009-9587-4/METRICS.

[13] G.J. Pielak, Buffers, Especially the Good Kind, Biochemistry. 60 (2021) 3436–3440. https://doi.org/10.1021/ACS.BIOCHEM.1C00200/ASSET/IMAGES/LARGE/BI1C00200_0002.JPEG.

[14] H.H. Li, Refractive index of alkaline earth halides and its wavelength and temperature derivatives, J. Phys. Chem. Ref. Data. 9 (1980) 161–290. https://doi.org/10.1063/1.555616.

[15] J.E. Bertie, Z. Lan, Infrared Intensities of Liquids XX: The Intensity of the OH Stretching Band of

Liquid Water Revisited, and the Best Current Values of the Optical Constants of H_2O(l) at 25°C between 15,000 and 1 cm^{-1}, Appl. Spectrosc. 50 (1996) 1047–1057. https://doi.org/10.1366/0003702963905385.

[16] J.-J. Max, C. Chapados, Isotope effects in liquid water by infrared spectroscopy. III. H_2O and D_2O spectra from 6000 to 0 cm^{-1}., J. Chem. Phys. 131 (2009) 184505. https://doi.org/10.1063/1.3258646.

[17] K. Yamamoto, H. Ishida, Optical theory applied to infrared spectroscopy, Vib. Spectrosc. 8 (1994) 1–36. https://doi.org/10.1016/0924-2031(94)00022-9.

[18] J.M. Chalmers, N.J. Everall, Qualitative and Quantitative Analysis of Plastics, Polymers and Rubbers by Vibrational Spectroscopy, in: Handb. Vib. Spectrosc., John Wiley & Sons, Ltd, 2007. https://doi.org/10.1002/9780470027325.s6101.pub2.

[19] P.R. Griffiths, J.A. De Haseth, Fourier transform infrared spectrometry, Wiley-Interscience, 2007. https://www.wiley.com/en-es/Fourier+Transform+Infrared+Spectrometry,+2nd+Edition-p-9780471194040 (accessed June 28, 2019).

[20] H.M. Heise, Improvements in the determination of cell parameters from the interference measurement by an IR-spectrometer, J. Mol. Struct. 114 (1984) 291–296. https://doi.org/10.1016/0022-2860(84)87147-1.

[21] G. Kraus, G. Gauglitz, Application and comparison of algorithms for the evaluation of interferograms, Fresenius. J. Anal. Chem. 344 (1992) 153–157. https://doi.org/10.1007/BF00322701.

[22] C.Y. Tan, Y.X. Huang, Dependence of Refractive Index on Concentration and Temperature in Electrolyte Solution, Polar Solution, Nonpolar Solution, and Protein Solution, J. Chem. Eng. Data. 60 (2015) 2827–2833. https://doi.org/10.1021/acs.jced.5b00018.

[23] D.R. Lide, CRC Handbook of Chemistry and Physics, 96th ed., CRC Press, 2015.

[24] W.J. Ferguson, K.I. Braunschweiger, W.R. Braunschweiger, J.R. Smith, J.J. McCormick, C.C. Wasmann, N.P. Jarvis, D.H. Bell, N.E. Good, Hydrogen ion buffers for biological research, Anal. Biochem. 104 (1980) 300–310. https://doi.org/10.1016/0003-2697(80)90079-2.

[25] R. Swanepoel, Determination of the thickness and optical constants of amorphous silicon, J. Phys. E. 16 (1983) 1214. https://doi.org/10.1088/0022-3735/16/12/023.

Supporting Information to

Nanometric determination of the thickness of aqueous samples for accurate molar absorption coefficients of water-soluble molecules in the mid-infrared region

Mónica V. Gutierrez-Salazar, and Victor A. Lorenz-Fonfria*

Institute of Molecular Science, Universitat de València, 46980 Paterna, Spain.

*Corresponding Author. E-mail: victor.lorenz@uv.es

Supplementary Figures

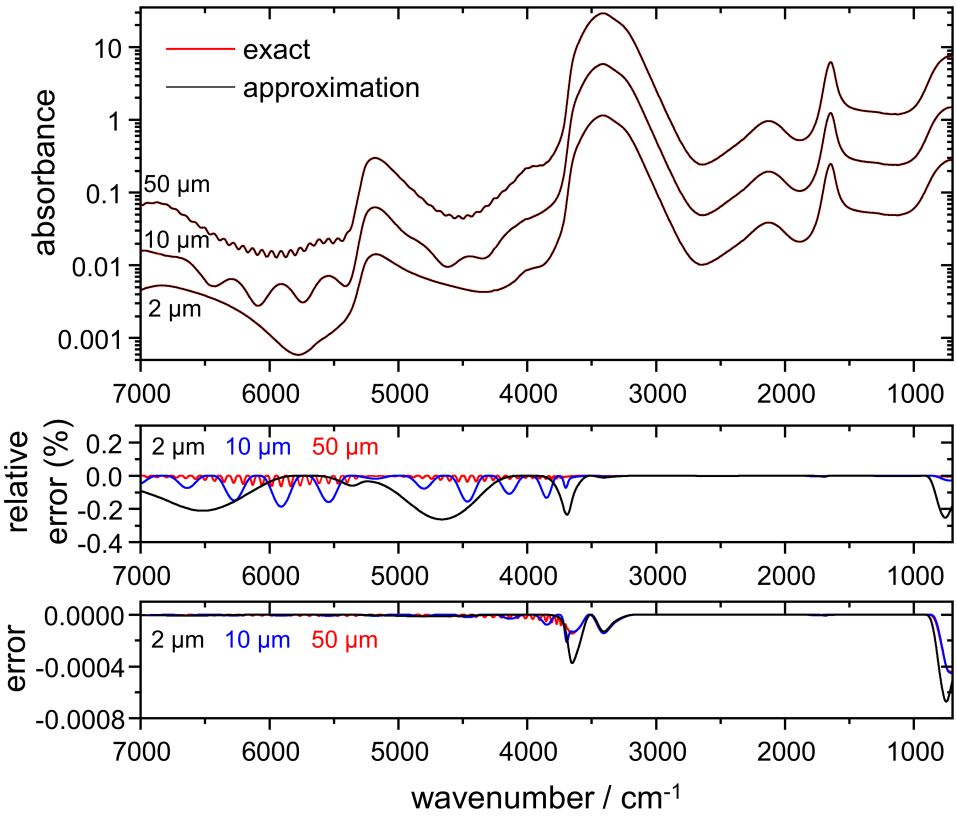

Figure S1. Calculated absorption spectra of liquid H_2O between CaF_2 windows in a transmission experiment for three different sample thicknesses, using either an exact (red) or an approximate (back) analytical expression (Top) derived from Fresnel equations and using optical constants of liquid H_2O from Bertie and Lan [1]. Note that the absorbance is presented in logarithmic scale for better comparison. Relative (Middle) and total (Bottom) error made when using the approximate expression for three different thicknesses.

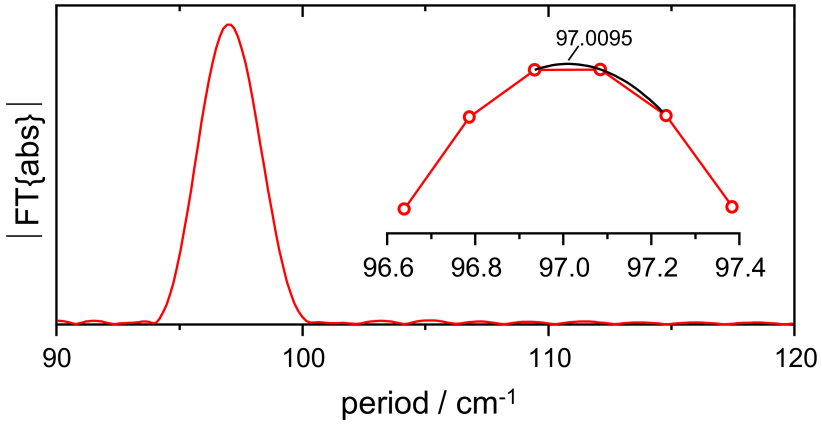

Figure S2. Magnitude of the Fourier transform of the interference fringes of an empty cell (see Fig. 3d in the MS). The insertion shows the actual data points after the Fourier transform as hollow circles. The peak position, i.e, the period of the interference fringes, is determined analytically after fitting a second order polynomial to the three most intense points of the peak (black trace).

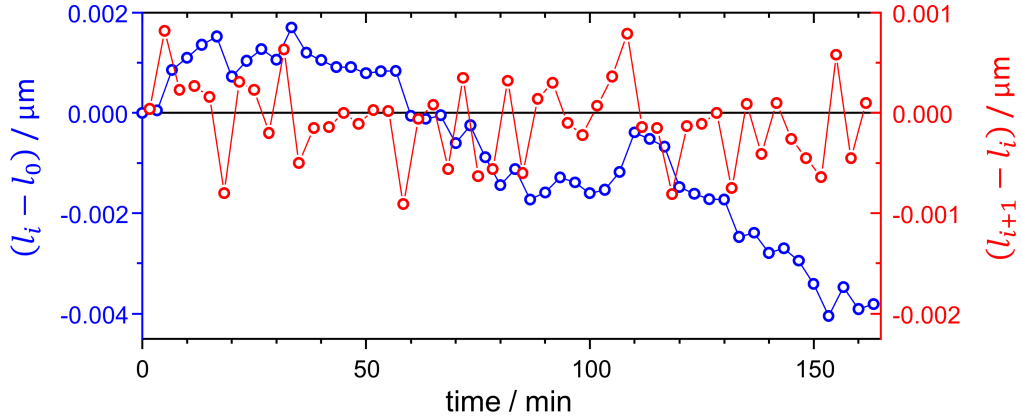

Figure S3. Variability of the estimated sample pathlength of an empty cell of 50 µm nominal thickness for multiple measurements extending for almost 170 min to respect the first measurement (blue trace). Variability of the estimated sample pathlength from one measurement to next measurement (red trace).

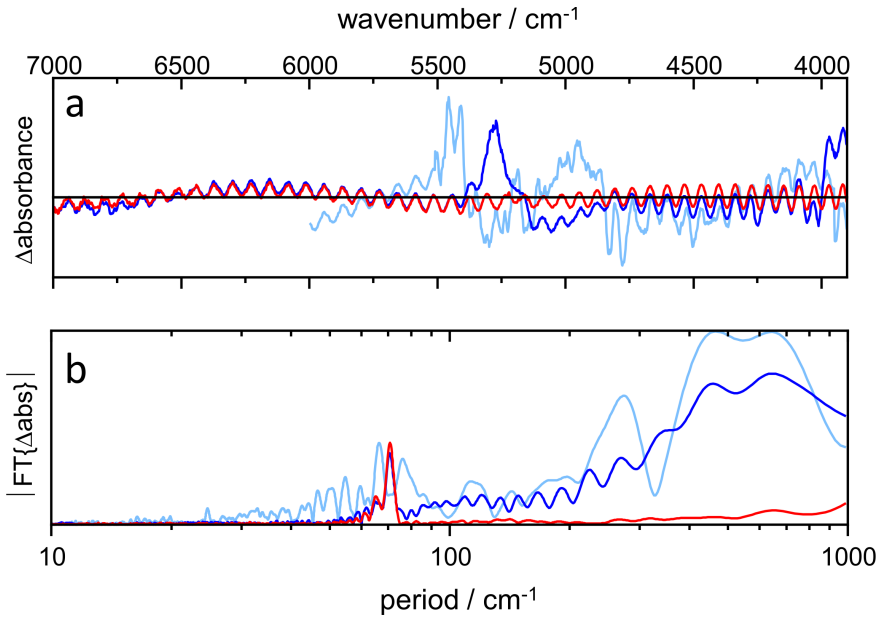

Figure S4. Revealing interference fringes in an absorption spectrum of liquid water after subtracting water contributions. (a) For the subtraction of water contributions we used either the molar absorption coefficient spectra from Max and Chapados [2] (light blue trace) or from Bertie and Lan[1] (blue trace), or we subtracted an experimental absorption spectrum of liquid water measured in a thicker cell (see Fig. 7 from the MS for more details). (b) Magnitude Fourier transform of the spectra in (a). Note that the subtraction of an experimental absorption spectrum provides the best results.

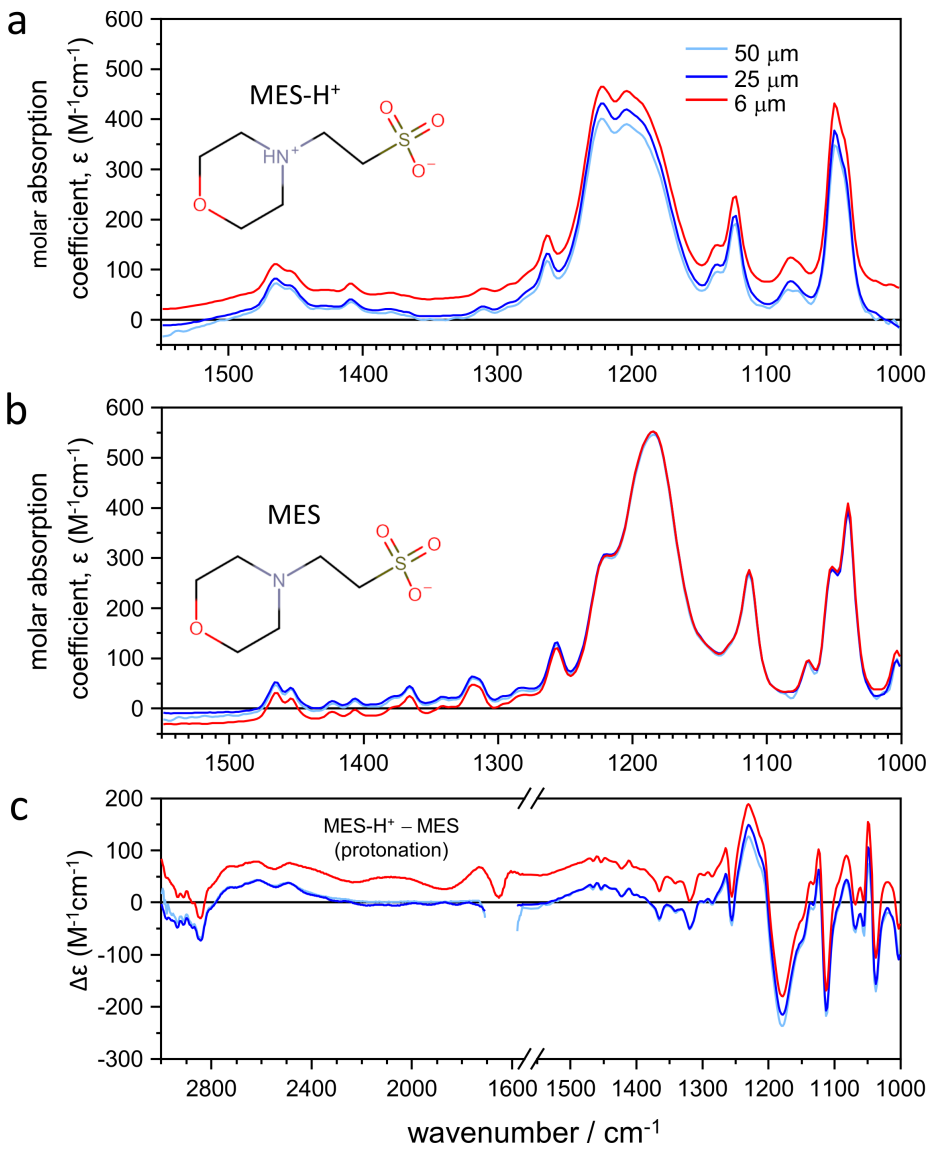

Figure S5. Raw estimation of molar absorption coefficient spectra of MES from absorption spectra recorded in cells with nominal thicknesses of 50, 25 and 6 μm. (a) Molar absorption coefficient spectra for the acidic form of MES calculated from samples of different thicknesses. (b) Same as (a), but for the basic form of MES. (c) Difference molar absorption spectra between the acidic and basic forms of MES, representing MES protonation (color-coded as in (a)).

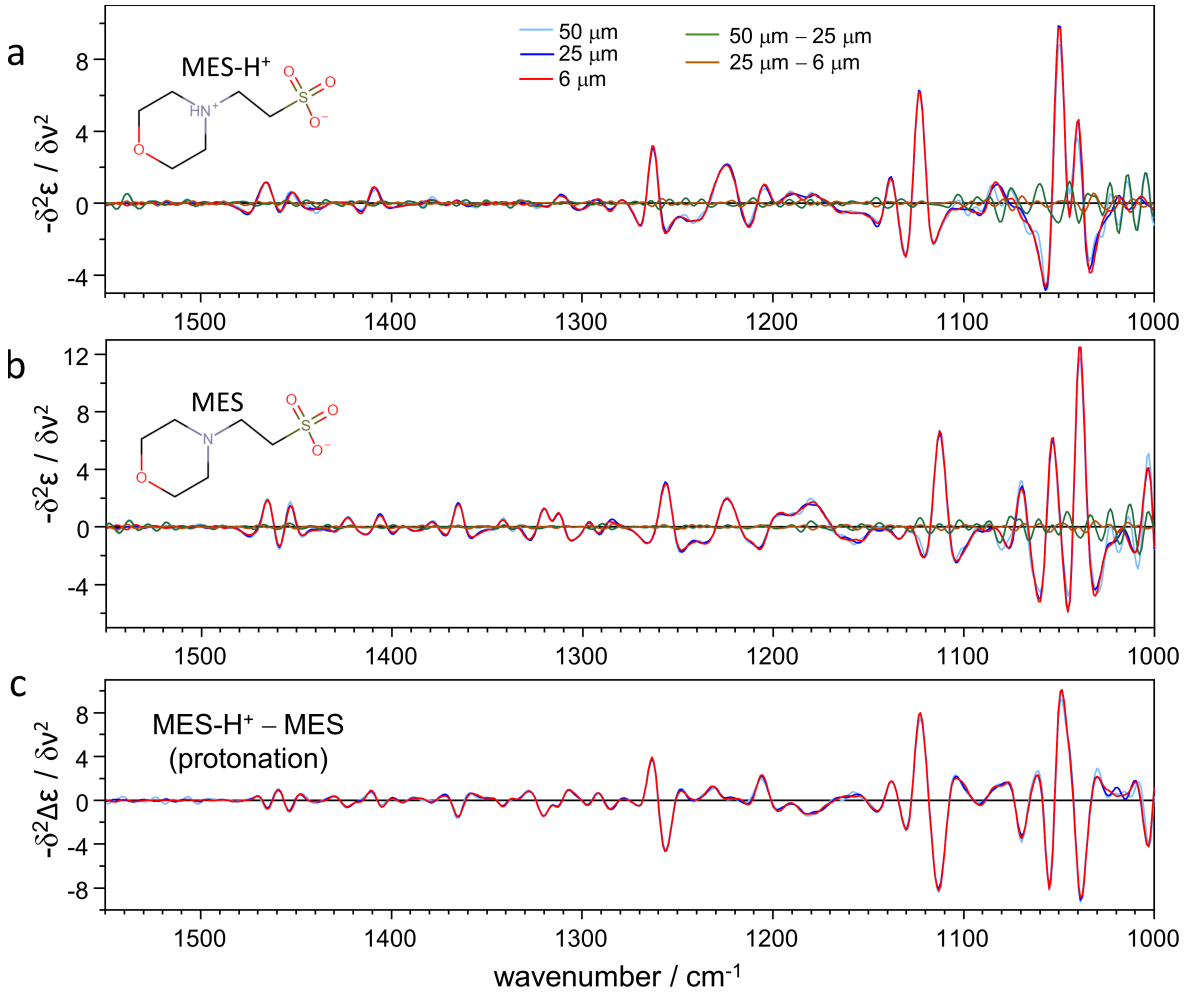

Figure S6. Minus second derivative a of the raw molar absorption coefficient spectra of MES from Fig. S5. (a) Minus second derivative molar absorption coefficient spectra for the acidic form of MES calculated from samples of different thicknesses. The difference between the estimate obtained with cells of two thicknesses (50 and 25 μm, and 25 and 6 μm) shows that the estimates do not differ in their scaling (i.e., their pathlength was correctly estimated) but differ due to noise, larger below 1100 cm^{-1} because of the background absorption of CaF_2 and water at this region (b) Same as (a), but for the basic form of MES. (c) Minus second derivative of the difference molar absorption spectra between the acidic and basic forms of MES, representing MES protonation (color-coded as in (a)). The second derivative was calculated in the Fourier domain as described [3,4], using a resolution of 4 cm^{-1} and a $Sinc^2$ apodization.

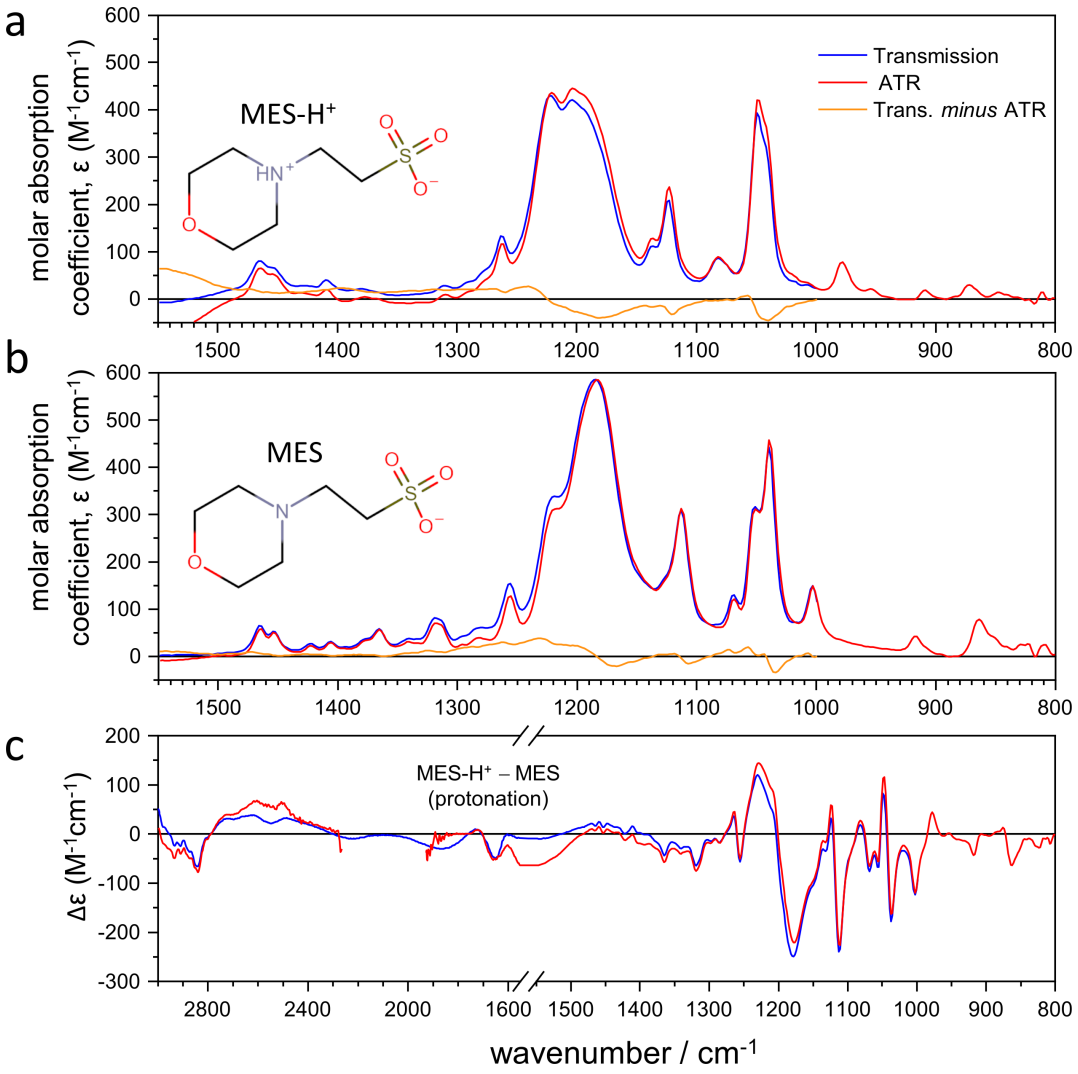

Figure S7. Comparison of molar absorption coefficient spectra for the buffer MES obtained from transmission spectroscopy (reproduced from Fig. 10 in the MS) and obtained previously by attenuated total reflection (ATR) spectroscopy.[5] (a) Molar absorption coefficient spectra for the acidic form of MES from transmission (blue) and ATR (red). (b) Same as (a), but for the basic form of MES. In (a) and (b) we show the difference between the estimation by transmission and by ATR spectroscopy (orange), with clear discrepancies for the most intense peaks. (c) Difference molar absorption spectrum between the acidic and basic forms of MES, representing MES protonation, color-coded as in (a).

References

[1] J.E. Bertie, Z. Lan, Infrared Intensities of Liquids XX: The Intensity of the OH Stretching Band of Liquid Water Revisited, and the Best Current Values of the Optical Constants of H_2 O(l) at 25°C between 15,000 and 1 cm^{-1}, Appl. Spectrosc. 50 (1996) 1047–1057. https://doi.org/10.1366/0003702963905385.

[2] J.-J. Max, C. Chapados, Isotope effects in liquid water by infrared spectroscopy. III. H_2O and D_2O spectra from 6000 to 0 cm^{-1}., J. Chem. Phys. 131 (2009) 184505. https://doi.org/10.1063/1.3258646.

[3] V.A. Lórenz-Fonfría, E. Padrós, Curve-fitting of Fourier manipulated spectra comprising apodization, smoothing, derivation and deconvolution., Spectrochim. Acta. A. Mol. Biomol. Spectrosc. 60 (2004) 2703–10. https://doi.org/10.1016/j.saa.2004.01.008.

[4] D.G. Cameron, D.J. Moffatt, A Generalized Approach to Derivative Spectroscopy, Appl. Spectrosc. 41 (1987) 539–544. https://doi.org/10.1366/0003702874448445.

[5] V.A. Lorenz-Fonfria, M. Saita, T. Lazarova, R. Schlesinger, J. Heberle, pH-sensitive vibrational probe reveals a cytoplasmic protonated cluster in bacteriorhodopsin., Proc. Natl. Acad. Sci. U. S. A. 114 (2017) E10909–E10918. https://doi.org/10.1073/pnas.1707993114.